Sustainable Energy & Fuels

ROYAL SOCIETY OF CHEMISTRY

REVIEW

View Article Online
View Journal | View Issue

Cite this: *Sustainable Energy Fuels*, 2024, **8**, 4039

Graphene-based 2D materials for rechargeable batteries and hydrogen production and storage: a critical review

Chandra Sekhar Bongu, Sehar Tasleem, Mohan Raj Krishnan and Edreese Housni Alsharaeh *

Batteries and hydrogen energy devices are considered the most critical technologies for achieving zero carbon dioxide emissions. However, they still suffer from several limitations, including low efficiency, short cycling life, low storage, and poor safety. With their strong mechanical strength (flexibility), chemical inertness, large surface area, remarkable thermal stability, and excellent electrical and high ion conductivity, graphene can overcome some of the issues associated with batteries and hydrogen energy devices. The properties of various two-dimensional (2D) materials make them potential candidates for a wide range of applications (batteries and hydrogen energy devices), thereby gaining considerable interest. Similarly, graphene has the potential for efficient hydrogen production and storage because of its large surface area and adjustable porosity. Graphene/2D composite materials are promising electrodes for lithium batteries, hydrogen storage, and production applications. This review provides a comprehensive overview of graphene/2D composite materials for lithium batteries and hydrogen storage and production applications.

Received 15th April 2024
Accepted 28th July 2024

DOI: 10.1039/d4se00497c

rsc.li/sustainable-energy

1. Introduction

The expanding population and growing industrialization have increased the need for energy globally to an unprecedented degree. However, most of our energy comes from fossil fuels, which increase greenhouse gas emissions (GHGs) and contribute to worldwide climate change.[1–4] The rising temperature of the earth's has prompted scientists to explore alternative energy sources. Reducing the dependency on fossil fuels and utilizing renewable energy to build new technologies are urgent. As a result, hydrogen (H_2) and batteries are considered clean and sustainable energy sources for the future.[5–12]

Batteries can store intermittent energy; thus, they are becoming increasingly popular as renewable sources.[13–15] Lithium-ion batteries are the most researched rechargeable batteries owing to their excellent energy density and storage capacity, which are advantageous for various applications and daily energy demands.[16–21] Electrode materials are crucial to lithium rechargeable batteries, but the sluggish kinetics and significant volume changes still hinder further applications.[16,22–24]

H_2 is an effective and clean energy source that substitutes fossil fuels.[25–27] Hydrogen energy has a gravimetric density roughly seven times higher than that of fossil fuels.[28] Hydrogen, a readily available element and a flexible energy carrier, can transform several industries and sectors, including manufacturing, transportation, and power generation. The potential of hydrogen to provide energy without producing hazardous pollutants makes it significant. Since water is the only byproduct of using hydrogen as fuel, hydrogen is a clean and green choice.[29] However, even with its enormous promise, there are still some obstacles that must be overcome before hydrogen energy is widely used.[30] The main issues are linked to the production and storage of H_2 energy.[31] Regarding H_2 production, novel catalysts and materials, such as nanostructured catalysts, are being investigated to speed up reactions and increase the efficiency for maximizing hydrogen generation.[29] Furthermore, the lower volumetric density of hydrogen necessitates huge storage capacities or high pressure. Therefore, advanced catalysts and materials can significantly improve the efficacy and effectiveness of hydrogen storage.[32] The common materials used to store hydrogen energy are sodium aluminium hydride ($NaAlH_4$), lithium aluminium hydride ($LiAlH_4$), lithium borohydride ($LiBH_4$), magnesium nickel hydride (Mg_2NiH_4), sodium borohydride ($NaBH_4$), aluminium hydride (AlH_3), zeolites, metal–organic frameworks (MOFs), and covalent organic frameworks (COFs).[33–40] However, the drawback of hydrogen adsorption–desorption exists as it lacks reversibility because of its strong bonding force and slow kinetics, necessitating high temperatures for desorption. For the production of hydrogen, titanium dioxide (TiO_2), molybdenum disulfide (MoS_2), tungsten(VI) oxide (WO_3), zinc oxide (ZnO), iron oxide (α-Fe_2O_3), bismuth vanadate ($BiVO_4$), copper

College of Science and General Studies, AlFaisal University, PO Box 50927, Riyadh, 11533, Saudi Arabia. E-mail: ealsharaeh@alfaisal.edu

oxide (Cu_2O), cadmium sulfide (CdS), and copper/zinc/tungsten (Cu/Zn/W) sulfide are widely employed as electrodes.[41–48] However, certain stability and low-efficiency challenges persist, leading to their poor photoelectrochemical (PEC) activity for hydrogen production.[49,50] Thus, innovative strategies are needed to address these issues and increase hydrogen generation methods' safety, economy, and efficiency.

Lithium-ion batteries, hydrogen storage, and production electrode material capabilities are found in several carbon-based substrates including porous carbons (PCs), carbon nanotubes (CNTs), MXenes and nanofibres (NFs) with different geometries.[51–56] Among all the recently discovered and synthesized nanostructured carbonaceous species, graphene stands out as the most extraordinary material. Their remarkable properties including their enormous surface area, mechanical toughness, and electrical conductivity have revolutionized the study of materials. Consequently, compared to other carbon compounds (PCs, CNTs, MXenes, and NFs), graphene has been used advantageously as prospective substitute electrode materials in many applications for improving particular technical domains, particularly those related to energy generation and storage. Because of their large theoretical SSA (2630 $m^2 g^{-1}$) and ease of functionalization by heteroatoms such as N atoms, graphene offers more electrochemical reaction active sites than other carbon compounds (PCs, CNTs, MXenes, and NFs).

Graphenes were isolated in 2004 and used in energy storage due to their high thermal conductivity, high electrical conductivity, high elasticity and flexibility, and high hardness. Particularly in lithium-ion batteries, they serve as electrodes, conductive materials, and controllers for volume expansion in the electrode material. However, Li ions may ideally be accommodated on both sides of graphene, and their theoretical capacity is at least double that of other carbon-based materials (PCs, CNTs, MXenes, and NFs).[57,58] The graphene is a promising substitute for improving H_2 generation efficiency. Because of graphene's particular two-dimensional conjugated framework and electrical characteristics, it can be used to increase the photocatalytic efficiency.[59] Moreover, the graphene, composed of carbon atoms arranged in a honeycomb lattice, holds the potential for hydrogen storage, giving rise to new hopes for creating an effective solid-state hydrogen storage device.[60] In recent years, several papers have been published on graphene composites with 2D materials in batteries and hydrogen storage and production applications. This review aims to assess graphene composites with 2D materials for lithium batteries, hydrogen storage, and production applications.

2. Lithium rechargeable batteries

2.1 Graphene-based 2D materials for lithium-ion batteries (LIBs)

2.1.1. Graphenes for lithium-ion batteries (LIBs). Numerous portable devices that are essential to modern life are powered by rechargeable batteries. Rechargeable battery technologies with high power and energy densities are also currently being investigated for the electrification of autos.[61,62] The market for rechargeable batteries used for energy storage is dominated by LIBs, a type of battery that operates on the intercalation and de-intercalation of Li ions due to many fascinating features, such as high energy and power density, long cycle life, low self-discharging, and no memory effect.[63] As seen in Fig. 1, lithium-ion batteries typically consist of the following four components: the cathode, anode, electrolyte, and separator.[64] Graphitic materials are typically used as the anode material in commercial LIBs, while Li metal oxides or phosphates such as $LiCoO_2$ and $LiFePO_4$ are commonly used as the cathode material.[65] A separator keeps the chemical potentials of the cathode and anode apart. During the charging and discharging processes, Li ions can flow between the cathode and the anode *via* an organic electrolyte based on carbonate, including a salt containing Li, such as lithium hexafluorophosphate ($LiPF_6$). During discharging, electrons move from the anode to the cathode while Li ions move through the electrolyte to keep the charge balanced. An external electrical power source forces the electrons and Li ions to go in the opposite direction during the charging process.

"Anode" refers to the negative electrode that releases an electron into the external circuit. An anode collects lithium ions and converts them into active materials. Some characteristics that the anode materials should have include a large energy capacity, excellent charge/ion storage, ion release, long cycle rate, ease of manufacture, safety in use, and cost-effectiveness.[67] Since the early 1990s, Sony has been commercially launching LIBs, with graphite was the anode material. Currently, graphite, the most popular anode material in LIBs, has a relatively low theoretical capacity of about 372 mA h g^{-1} and safety issues related to the insertion of Li^+ into the anode structure.[68] A graphite anode's limited capacity will prevent it from meeting the demands of the rapidly expanding industries.[69] To improve LIB performance and energy density, research is required to fabricate new anode materials with a capacity greater than that of graphite.[70]

A 2D nanomaterial called graphene is made up of hexagon-shaped carbon atoms with sp^2 hybrid orbitals. Graphene has garnered considerable interest across numerous applications since its isolation in 2004.[71–77] Graphene, a single layer of

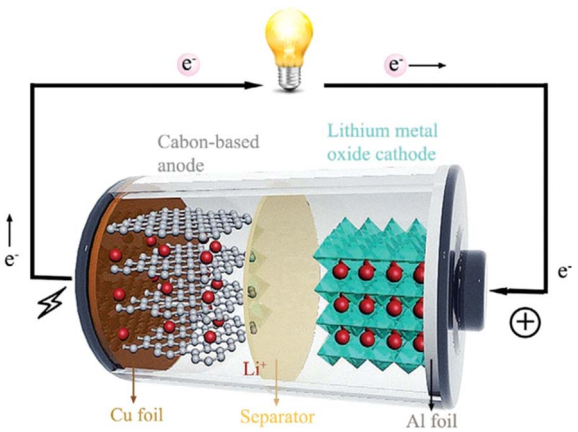

Fig. 1 Schematic of the structure and working mechanism of LIBs.[66]

graphite, is attracting a lot of attention as a potential anode material due to its enormous specific surface area (2620 m^2 g),[78] mechanical strength, excellent thermal conductivity (5000 W m^{-1} K^{-1}),[79] electrical conductivity, rapid charge–discharge cycles and a more remarkable ability to hold Li ions and higher capacity (three times that of graphite).[80–83] Because of its high energy storage capacity of 669 mA h g^{-1}, good cycling stability, longer interlayer distance of 0.615 nm with mild van der Waals forces, and simple intercalation and deintercalation procedure, graphene is highly suitable for LIB anode applications.[84] Numerous scientists have noted that Li^+ ion attachments may be facilitated by extra paths provided by graphene sheet defects. The enormous challenge of fabricating LIBs that can provide high power and energy density outputs during charging and discharging may have an answer in this feature. However, porous graphene's high ionic conductivity, surface characteristics, and electric conductivity have attracted considerable attention in battery research.[85] Ordered mesoporous graphene nanosheets were synthesized by Fang *et al.* using a regulated low-concentration mono micelle close-packing assembly technique.[86] This anode can hold 833 mA h g^{-1} at different current densities after multiple cycles. It can give a high reversible capacity of 1040 mA h g^{-1} at 100 mA g^{-1}. About 255 mA h g^{-1} of reversible capacity is kept even at a high current density of 5 A g^{-1}. For instance, magnesium oxide and methane were used as starting ingredients in the chemical vapor deposition process to synthesize a hierarchical porous graphene nanomaterial. The Brunauer–Emmett–Teller (BET) surface area and pore size were changed, and this affected the electrochemical properties of LIBs.[87] In particular, the heteroatom-doped graphene has demonstrated advances in the electrochemical performance of LIBs. Using the differential electroneutrality of doped nitrogen (N), phosphorus (P), sulfur (S), and boron (B) heteroatoms, a method was devised to increase the relative specific capacity (900 mA h g^{-1}) of LIBs.[81,88–92] However, extensive research has revealed that the ionic-steric effect and decreased stability of graphene make it impractical to use it directly as an anode active material in LIBs.[93,94] Furthermore, with several advantageous effects, the synthesis of graphene-based composites has been one of the most important avenues for LIB anode active materials. The graphene, particularly with a 2D material, has emerged as a potential anode active material for LIB applications.

2.1.2. Graphene/graphitic carbon nitride (C_3N_4) anodes for lithium-ion batteries. Because of their comparable layered architectures, graphene and graphitic carbon nitride (C_3N_4) are known to be modifiable. Synergistic effects between graphene and g-C_3N_4 are caused by highly exposed N-active sites on conductive graphene sheets, which increase the electrochemical characteristics. Nevertheless, these active spots become inactive as soon as graphene aggregation occurs. Thus, structural exploration of g-C_3N_4/graphene-based materials could help design a stable 2D structure with many active sites. Shuguang Wang *et al.* prepared a g-C_3N_4@reduced graphene oxide composite (g-C_3N_4@RGO) in a cost-effective way and applied it as an LIB anode (Fig. 2a).[95] For practical applications, the coin-type half batteries are fabricated with g-C_3N_4@RGO and connected in series to a tandem red light-emitting diode (LED) and a watch. The g-C_3N_4@RGO electrode delivered a stable cycle performance with a 595.1 mA h g^{-1} capacity even after 1000 cycles at a high current density of 1 A g^{-1}. Marlies Hankel and co-workers designed a C_3N_4/graphene heterostructure and conducted scanning electron microscopy (SEM) analysis to observe its morphology (Fig. 2b). However, the Density Functional Theory (DFT) study showed superior conductivity of the designed C_3N_4/graphene heterostructure for LIB applications. The C_3N_4/graphene heterostructure electrode exhibited an excellent electrochemical capacity of 862.2 mA h g^{-1} after 90 cycles with a coulombic efficiency of 90.4%.[96]

2.1.3. Graphene/hexagonal boron nitride (h-BN) for lithium-ion batteries. With its strong mechanical strength, chemical inertness, remarkable thermal stability, and high ion conductivity, h-BN has emerged as a potential solution for various energy storage and conversion issues. Generally speaking, h-BN can function as an ideal modifier to increase battery safety by enhancing separators' mechanical strength, providing superior thermal conductivity, and prolonging the cycle life of Li-metal batteries by safeguarding the solid-state electrolyte. During charge–discharge cycling, lithium metal experiences a constant growth of Li dendrites, which results in low coulombic efficiency and early failure. After extensive cycle experiments, John Hong *et al.* reported a freestanding h-BN nanosheet separator with exceptional physical rigidity against dendritic Li development and exceptional thermal endurance in high-temperature settings.[100] Pol *et al.* prepared bilayer separators and used them in lithium-ion batteries. A polypropylene (PP) membrane covered with a layer of boron nitride-graphene (BN_xGr_y) dramatically lowers polarization and impedance while greatly enhancing cell performance and stability. The full cell fabricated with the modified BN_xGr_y/PP separator delivered a discharge capacity of 114 mA h g^{-1} at 1C rate even after 1000 cycles (Fig. 2e).[97] Using the Hall potentiometry approach, Frank Zhao *et al.* reported the electrochemical intercalation of Li into graphene enclosed between h-BN layers (Fig. 2c).[98] This work presents an electrochemical method for the controlled intercalation of lithium ions into a range of van der Waals heterostructures composed of hexagonal boron nitride and graphene. Tong Teo and colleagues successfully made the composite films of reduced graphene oxide (rGO)/boron nitride (BN) using simple vacuum filtration and subsequent heat treatment (Fig. 2d).[99] The thin 2D nanosheet morphologies of rGO and BN were well retained following their combination, according to the morphological analysis of the generated rGO/BN SEM images. The electrochemical analysis indicates that the composite film electrode with rGO/BN (rGO/BN-2%) exhibits superior rate performance. Even at a high current density of 1 A g^{-1}, the rGO/BN (rGO/BN-2%) electrode delivers a specific capacity of 121 mA h g^{-1}, which is higher than that of the rGO film electrode.

2.1.4. Graphene/transition metal dichalcogenides (TMDs) for lithium-ion batteries. Because of their unique lamellar structure, TMDs have a superior electrochemical active interface, excellent mechanical properties, higher specific capacity,

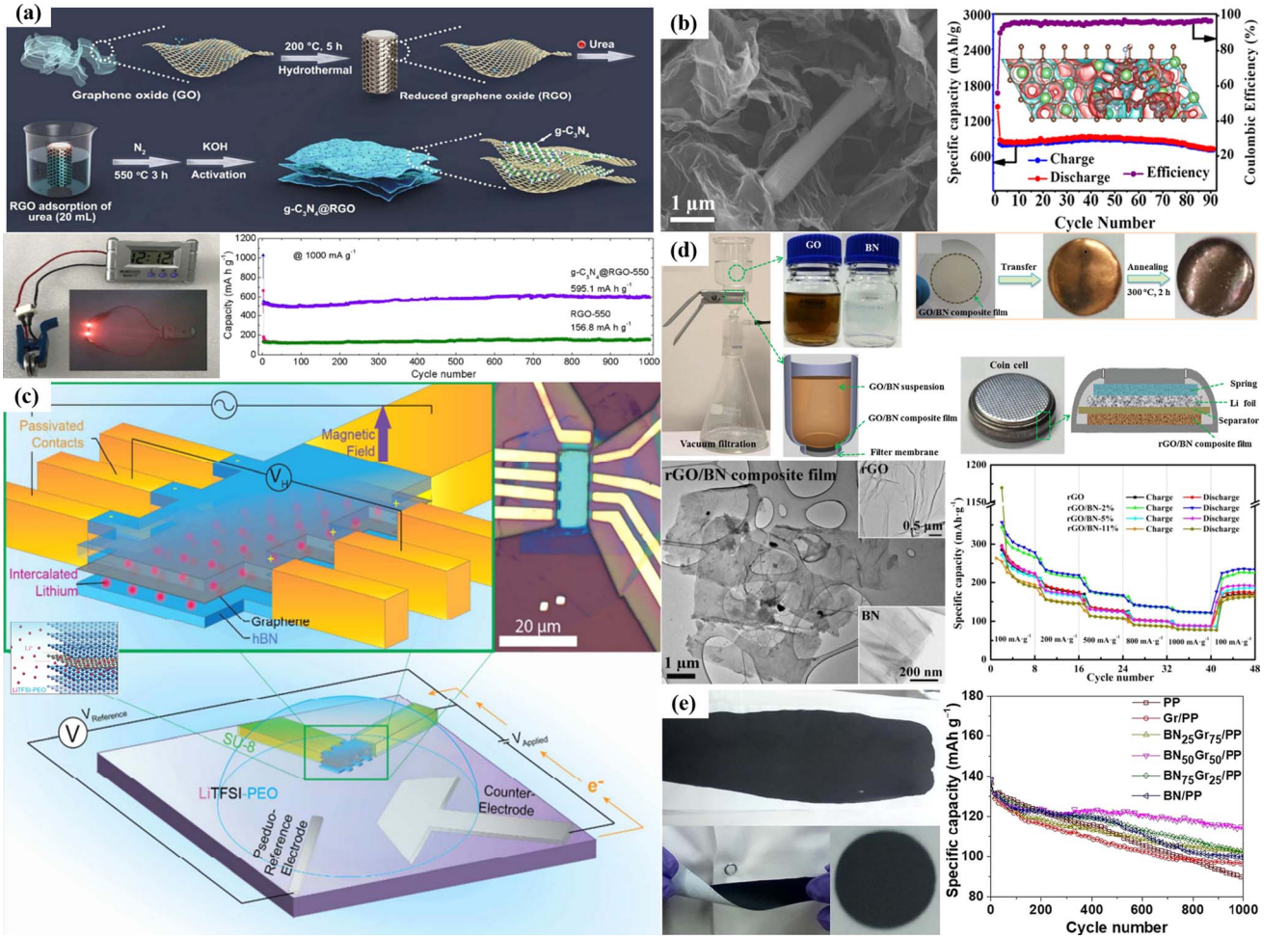

Fig. 2 (a) Schematic of the synthesis procedure of g-C_3N_4@RGO. (b) SEM image and DFT calculations of the C_3N_4/graphene heterostructure. (c) Hall bar device with the h-BN/graphene/h-BN heterostructure. (d) Vacuum filtration process for preparation, transmission electron microscopy (TEM) image and electrochemical study of the GO/BN composite film. (e) Bilayer BN_xGr_y/PP separator and electrochemical characterization of LIBs.[95–99]

and improved cycling stability compared to typical carbon anodes, and hence, LIBs frequently use them. However, TMDs are a viable option for energy storage applications because of their huge intercalation gap, which can encourage the quick interlayer migration of lithium ions. TMDs have the structure MX_2, where X can be either tellurium (Te), selenium (Se), or S, and M can be any transition metal element (*e.g.*, titanium (Ti), tungsten (W), vanadium (V), and molybdenum (Mo)). Typical two-dimensional TMDs are molybdenum disulfide (MoS_2), vanadium sulfide (VS_2), vanadium selenide (VSe_2), tungsten disulfide (WS_2), and so forth. The obstacles of the TMDs for commercial application volume expansion and during the charge–discharge process are the van der Waals interaction between TMD sheets, which lowers the utilization rate. TMDs with layered structures such as graphene are easier to exfoliate and facilitate quick ion diffusion. With its huge specific surface area, great mechanical capabilities, and excellent electrochemical stability, TMD/graphene heterogeneous composites are perfect energy storage materials. The hollow MoS_2 nanocages/RGO nanocomposites fabricated by Dafang He *et al.* are assembled using a straightforward solvothermal-assisted assembly technique in conjunction with freeze-drying and annealing (Fig. 3a).[101] The graphene and MoS_2 are tightly bound *via* molecular links, contributing to the structural stability, improved electrical conductivity, and increased lithium storage capacity of the MoS_2 anode material. Thus, at a high current density of 3 A g^{-1} (Fig. 3b), this new nanocomposite demonstrates good rate capability and significant potential as an anode nanocomposite for improved lithium-ion batteries. By a simple hydrothermal process, Xinglan Zhou *et al.* fabricated 1T MoS_2 nanosheets on graphene oxide (GO) as an anode in lithium-ion batteries. The synthesized 1T MoS_2/GO (1 g) electrode exhibited the first specific charging/discharging capacity of 1612 mA h g^{-1} at a current density of 0.1 A g^{-1}. It maintained a specific capacity of 774 mA h g^{-1} even after 60 cycles at a current density of 1 A g^{-1}.[105] WS_2 one more TMD was reported for lithium-ion battery anode materials due to its excellent electrochemical properties.[106] Yong-Lin Wu *et al.* synthesized a WS_2/graphene nanosheet composite *via* ball milling followed by calcination to overcome the van der Waals interactions

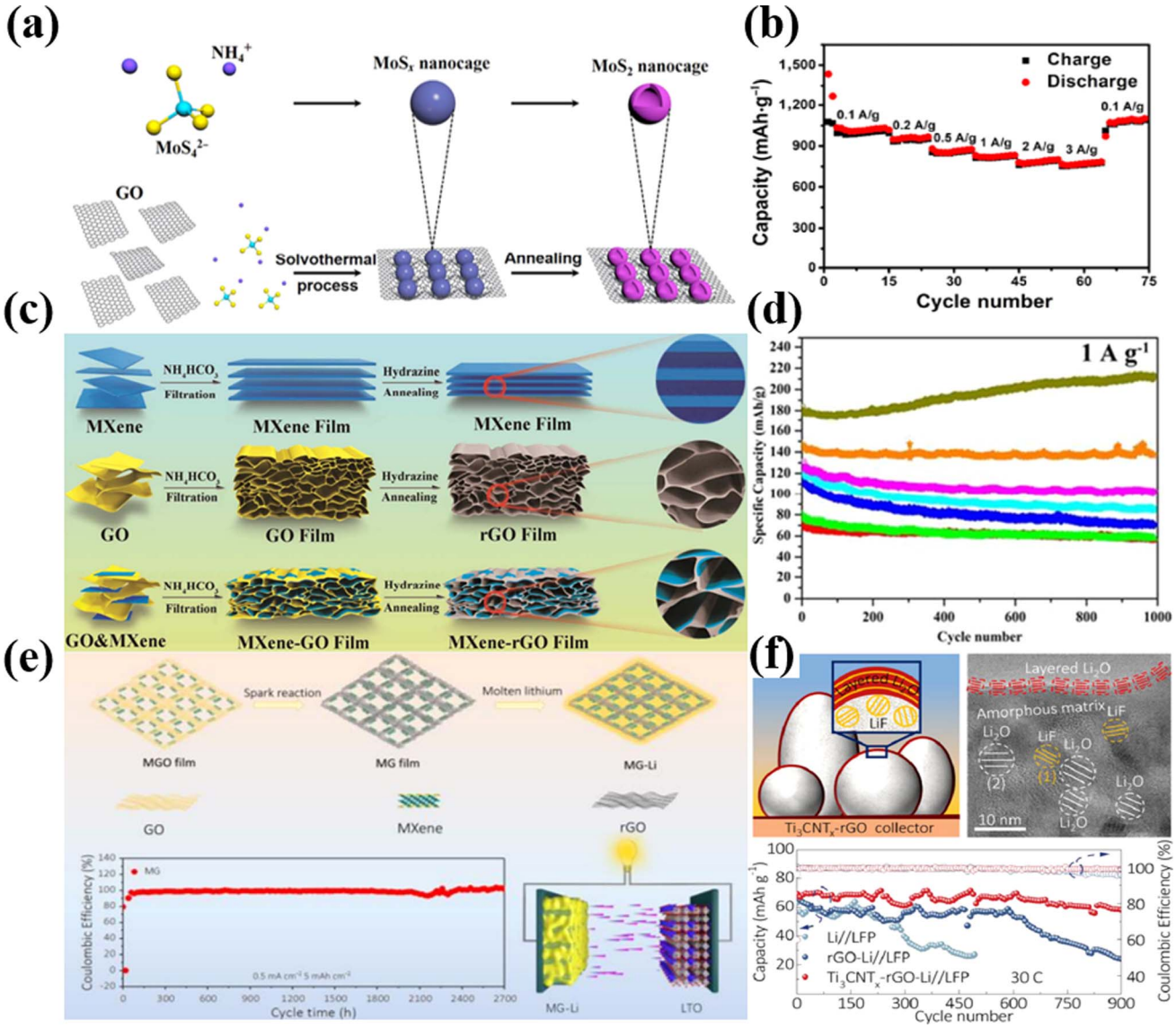

Fig. 3 (a) Synthesis process and (b) rate performance of the MoS_2/RGO nanocomposite and MoS_2 electrode. (c) Fabrication and (d) electrochemical performance of the MXene, rGO and MXene-rGO films at 1 A g^{-1}. (e) Fabrication and coulombic efficiencies of the MG electrode at a current density of 0.5 mA cm^{-2} with a Li deposition amount of 5 mA h cm^{-2} for 2700 h. (f) Lithiophilic functional groups result in the formation of a uniform SEI layer (decomposition of $LiN(CF_3SO_2)_2$); cryo-TEM images of equally dispersed LiF and ordered layered Li_2O and superior cycling lifespan over 900 cycles with a capacity retention of 77.7% at 30C of Ti_3CNT_x/G/Li electrode.[101–104]

between the interlayer of graphite and WS_2.[107] At a current density of 250 mA g^{-1}, the produced WS_2/GNS composite anode material exhibited a 95% capacity retention rate and a high reversible specific capacity of 705 mA h g^{-1} even after 200 cycles.

2.1.5. Graphene/MXenes for lithium-ion batteries. Another class of electrode materials that have recently attracted much attention are MXenes. MXenes is a collective term for a novel class of 2D carbonitride, nitride, and carbide materials that was coined in 2011. MXenes have demonstrated significant promise in using LIB electrodes due to their distinct 2D structure and abundant active sites on their surface. However, the noticeable restacking effects of MXene layers and low electric conductivity cannot be used in battery applications. Thus, MXenes combined with graphene composites have proven to be highly effective electrodes for Li-ion batteries, and they have been successfully fabricated. Yun-Ting Du *et al.* methodically examined the electrochemical characteristics of MXene/graphene heterostructures and their potential applications in energy storage through first-principles calculations.[108] The results show that adding graphene improves the mechanical stiffness, Li adsorption strength, and electric conductivity and prevents the restacking effects of MXene layers. Zhiying Ma *et al.* synthesized a MXene (titanium carbide (Ti_3C_2)) and graphene hybrid film in different ratios and applied it for lithium-ion storage applications (Fig. 3c).[102] The hybrid film has a high specific capacity of 335.5 mA h g^{-1} at 0.05 A g^{-1} and is used as an electrode material for lithium-ion batteries. Because of its stable structure, the film electrode also shows good cycling

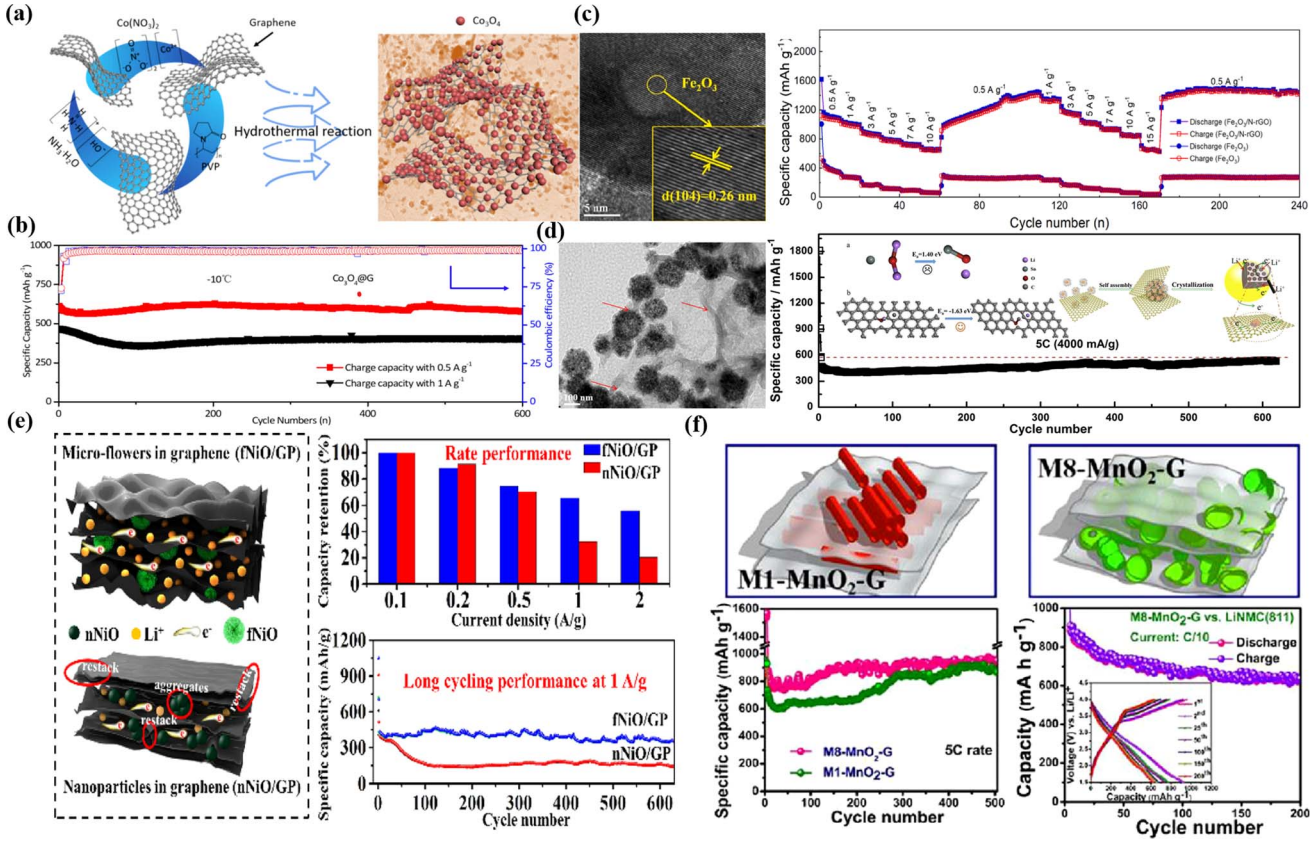

Fig. 4 (a) Schematic representation of the preparation and (b) long-cycling performance of Co_3O_4@G at −10 °C and different current rates. (c) High-resolution transmission electron microscopic (HRTEM) image of the Fe_2O_3/N-rGO sample and rate capability of Fe_2O_3/N-rGO and pure Fe_2O_3 at different current densities. (d) TEM image and long cycling performance of the SnO_2@graphene sponges (GS) at a current density of 5C. (e) NiO micro-flowers/graphene paper electrode rate capability at different current densities and long cycling at 1 A g^{-1}. (f) Long cycling performance of the M1-MnO_2-G and M8-MnO_2-G composite anode material and full cell study of the M8-MnO_2-G composite anode with the $LiNi_{0.8}Mn_{0.1}Co_{0.1}O_2$ cathode.[118–122]

stability, with no capacity loss even after 1000 cycles at high rates (1 A g^{-1}) (Fig. 3d). However, MXenes/graphene also use a dendrite-free Li metal anode in lithium-ion batteries. The synthesized MXene/graphene electrode by Zhong-Shuai Wu and colleagues has a record lifespan of 2700 hours and high coulombic efficiency of ~99% (Fig. 3e).[103] Comparably, the conductive scaffold was employed by MXene (Ti_3CNT_x) and graphene composites to control Li nucleation and solid-electrolyte interphase (SEI) production on the Li metal anode. With a capacity retention of 77.7% at 30C, the Ti_3CNT_x-G-Li electrode-based complete cells with $LiFePO_4$ have an exceptional cycling lifespan of over 900 cycles (Fig. 3f).[104] Carbon nanotubes (CNTs) and graphene with varying weight ratios of MXene to carbon, synthesized by Motahare S. Mohseni-Salehi *et al.*, were hybridized with the nanohybrids.[109] With a coulombic efficiency of 98%, the V_2CT_x MXene/G showed an impressive specific discharge capacity of 460 mA h g^{-1} at a current rate of 100 mA g^{-1}.

2.1.6. Graphene/transition metal oxides (TMOs) for lithium-ion batteries. Over the past few decades, transition metal oxides (TMOs) have been the subject of extensive research because of their intriguing charge transfer and storage properties. However, TMOs as LIB anodes are still far from commercial applications due to noticeable volume expansion (~300%) observed during the cycling process. To improve the anode material's performance and get around these problems, TMOs and graphenes can be combined.[110,111] The graphene is an ideal conductive carbon coating for TMO anode materials to mitigate the volumetric expansion.[112] Therefore, to overcome the aforementioned drawback, a number of methods have been proposed as practical solutions for extending the cycle life and reducing the volume expenditure of LIB anode materials. One such method is the preparation of nanocomposite materials, which capitalize on the synergy between combined materials.[113–116] By a straightforward sonication process, MnO_2 nanotubes were able to integrate the components *via* the electrostatic interaction of the MnO_2 nanotubes and graphene functional groups. It was discovered that the incorporation of graphene oxide improved the interfacial characteristics and structural stability during charge/discharge cycling while reducing volume expansion and charge transfer resistance.[117]

Cobalt oxide (Co_3O_4) has been studied as an anode material since it was first used as the anode electrode for LIBs because of its advantages, which include a large theoretical specific

capacity of approximately 890 mA h g^{-1}, wide availability, ease of manufacture, and stable chemical properties. Liang Tan *et al.* used a simple hydrothermal method to make a Co_3O_4/graphene composite, which was subsequently tested at very low temperatures (Fig. 4a).[118] The Co_3O_4/G anode exhibits a noticeably higher capacity of 605 mA h g^{-1} at 0.5 A g^{-1} (Fig. 4b) than that of other anodes at temperatures below zero thanks to the material's creative nanostructure, high conductivity, and extremely good lithiation and delithiation potentials. The inexpensive metal oxide Fe_2O_3 can displace graphite as the primary anode material for lithium-ion batteries. The redox conversion reaction from Fe_2O_3 to a combination of Li_2O and metallic iron gives a theoretical capacity of up to 1006 mA h g^{-1}. Yu Huang *et al.* used a simple and effective one-pot hydrothermal process to create a 2D nanostructured Fe_2O_3/N-rGO composite (Fig. 4c). When tested as LIB anodes, the 2D nanostructured Fe_2O_3/N-rGO composite demonstrated an exceptional high-rate capacity of 652 mA h g^{-1} at 15 A g^{-1} (Fig. 4c).[119] A similar Fe_2O_3/multilayer graphene was synthesized by Junming Xu *et al.* by a chemical deposition method, which when used as the anode for LIBs exhibited a specific capacity of 1050 mA h g^{-1} at 0.1C even after 100 cycles.[123] Due to their noteworthy characteristics, tin oxide (SnO_2) nanoparticles have been thoroughly investigated for various energy-related applications, including LIBs. Naiqing Zhang and coworkers reported hierarchical SnO_2 nanoclusters anchored on the graphene sponges (SnO_2/GS) *via* a solvothermal approach with an average diameter of ~110 nm, as shown in Fig. 4d.[120] These hierarchical SnO_2/GSs retained a higher reversible capacity of 600 mA h g^{-1} after over 600 cycles at 4000 mA g^{-1} (Fig. 4d). Based on a conversion reaction from nickel oxide (NiO) to metallic nickel and Li_2O, the estimated theoretical capacity for NiO is 718 mA h g^{-1}. The NiO also suffers from poor rate performance and cycling stability similar to those of other conversion-based anode nanomaterials. NiO composite with graphene is used in the LIB applications to address these obstacles. Ju Fu *et al.* synthesized hierarchically porous NiO micro-flowers/graphene papers (fNiO/GP) by a facile hydrothermal method followed by annealing in air at 400 °C for 40 min (Fig. 4e).[121] Even after 600 cycles at a current density of 1000 mA g^{-1}, fNiO/GP demonstrated high reversible specific capacities of 359 mA h g^{-1} in lithium-storage applications (Fig. 4e). Similarly, graphene–(Ni–NiO)–C hybrid was hydrothermally treated at 180 °C for 24 h and then carbonized at 700 °C for three hours by Jian-Guo Zhao and colleagues.[124] When it was used as the anode material for LIBs, the initial capacity was 711.6 mA h g^{-1}, and after 300 cycles, it increased to 772.1 mA h g^{-1}. Manganese dioxide (MnO_2) is plentiful in the Earth's crust, which is a more environmentally friendly metal oxide than other oxides. As an anode for LIBs, MnO_2 has a high theoretical capacity of 1232 mA h g^{-1}, enabling a quick charge/

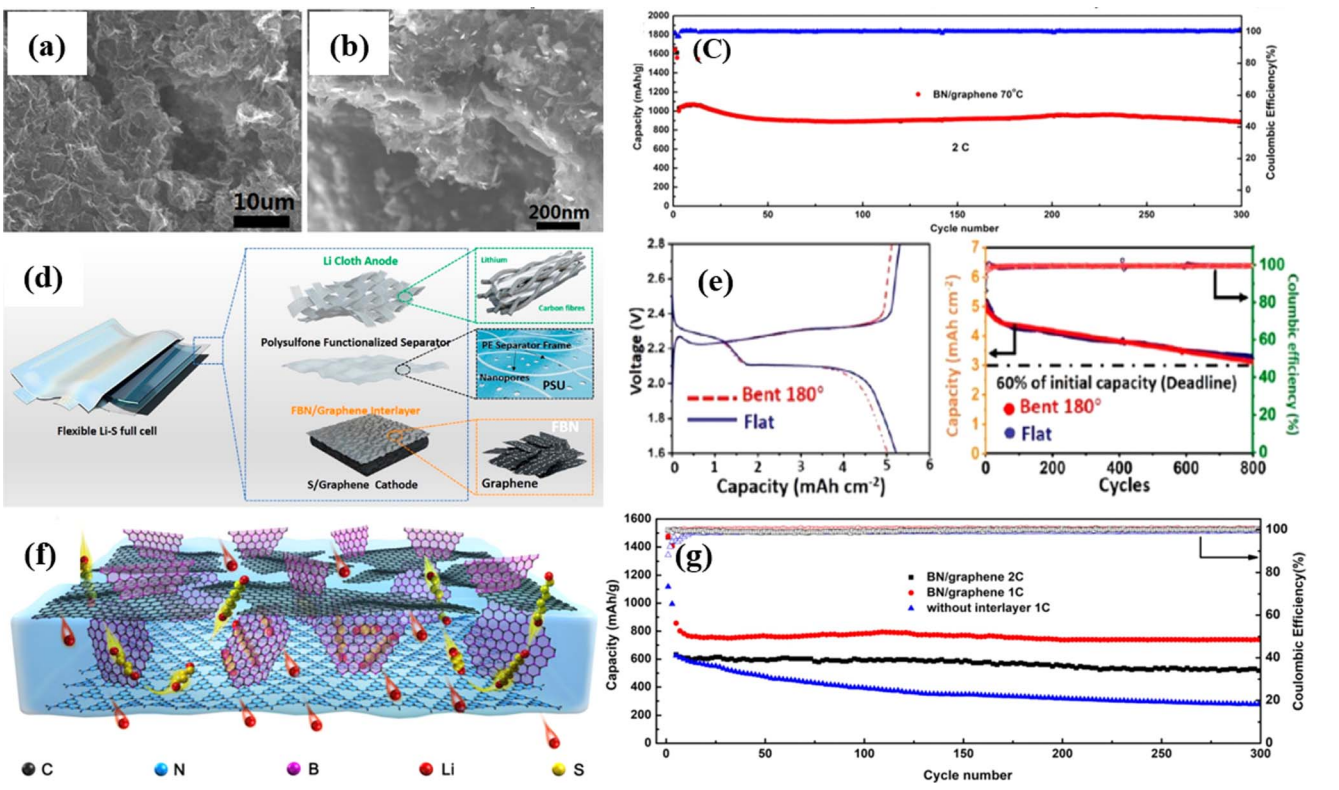

Fig. 5 (a and b) SEM images of BN/graphene. (c) Long cycling performance of BN/graphene at 70 °C temperature. (d) Lithium cloth anodes, PSU-Celgard separators, and free-standing graphene/sulfur cathodes shielded by an FBN/G interlayer are used to build flexible Li–S complete cells. (e) Charge/discharge curves and cycling performance of the Li–S pouch cells in the flat state and bent state, respectively, of the FBN/graphene interlayer. (f) Scheme of the multi-functional ion-sieve constructed by three 2D materials (gC_3N_4, BN and graphene). (g) Coulombic efficiency and discharge capacity of the cell with the BN/graphene interlayer at rates of 1C and 2C.[127–129]

discharge rate over a broad potential window. As anode materials for Li-ion batteries, Pedda Masthanaiah Ette *et al.* revealed that two distinct mesoporous MnO_2 were produced from silica templates (MCM-41 and MCM-48) and integrated with graphenes (Fig. 4f).[122] Both composites demonstrate improved rate performance, large discharge capacity, and strong cycling stability. When used as LIB electrodes, M8-MnO_2-G exhibits a consistent discharge capacity of 1494 mA h g^{-1} at a rate of 5C (Fig. 4f). The synergistic effects of graphene-integrated mesoporous MnO_2 are responsible for the composites' high specific capacities and long cycling performance. $LiNi_{0.8}Mn_{0.1}Co_{0.1}O_2$ as a cathode studied the full cell tests with an M8-MnO_2-G composite material anode. The full cell shows a stable capacity up to 200 cycles at a current density of 0.1C.[122]

2.2 Graphene-based 2D materials for lithium–sulfur batteries (LSBs)

Lithium–sulfur batteries are considered the most promising candidates among the battery technologies now used to act as the batteries of the future generation with superior electrochemical performance. The high specific capacity (~1675 mA h g^{-1}) and high energy density (~2600 W h kg^{-1}) of lithium–sulfur batteries (LSBs) have gained interest in recent years.[125] The present bottlenecks of LSBs include the severe shuttle effect of soluble lithium polysulfides (LiPSs) and slow redox kinetics, which lead to capacity fading and poor rate performance.[126] Due to the severe capacity fading (poor cycling stability) and low coulombic efficiency that these devices exhibit, the effective practical implementation of these devices has been put off. Numerous approaches have been proposed to address these problems, some of which involve using 2D-based materials to produce a better component architecture, as will be covered in the following discussion.

2.2.1. Graphenes/hexagonal boron nitride (h-BN) for lithium–sulfur batteries. With its Li-friendly surface and high stability, h-BN can reduce Li dendrites without sacrificing the Li-ion conductivity. Furthermore, h-BN can act as Lewis acidic sites to attract polysulfide anions in the electrolyte, increasing the Li–S battery capacity. Thanks to their synergistic impact, h-BN and graphenes have been validated as improved cathode materials in LSBs. This combination can efficiently adsorb LiPSs and speed up the redox kinetics for LiPS conversion, even under challenging conditions. According to Deng *et al.*, the G/BN composite cathode demonstrated a capacity fading <0.04% per cycle at 70 °C and reached a steady capacity of 888 mA h g^{-1} at 2C after 300 cycles. However, graphene/BN is also constituted by functional separators or interlayers blocking barriers for LiPS in LSBs. Recently, an extremely flexible LSB with a cathode made of graphene/sulfur composites, an anode made of lithium cloth, an interlayer made of functionalized BN nanosheets and graphenes, and a separator made of functionalized polysulfone have also been produced (Fig. 5a–c).

Consequently, the resulting flexible Li–S full-cells exhibit excellent electrochemical performance at a high areal capacity of 5.13 mA h cm^{-2} and a high volumetric and gravimetric energy density of 468 W h L^{-1} in the folded state, up to 800 cycles (Fig. 5d and e). In contrast to separators, an efficient interlayer must have a high conductivity to maximize the use of active sulfur and boost rate capability. With a polypropylene membrane covered with g-C_3N_4/h-BN/G, the LSB was built, and after 500 cycles at 1C, it released a discharge capacity of around 600 mA h g^{-1}. The capacity attenuation was less than 0.01% per cycle with a 6 mg cm^{-2} area S-loading (Fig. 5f and g).

2.2.2. Graphene/graphitic carbon nitride for lithium–sulfur batteries. The organic n-type visible light-active semiconductor graphitic carbon nitride (g-C_3N_4) photocatalyst attracted a lot of attention in various applications due to its 2D structure, composition devoid of metals, and excellent chemical and thermal stability. Strong affinity to Li_2S_n is demonstrated by graphitic carbon nitride (g-C_3N_4), a 2D structure similar to graphene, which is explained by the chemical interaction between Li atoms and pyridinic-N sites. Juan Zhang *et al.* used a microemulsion technique to fabricate a 3D porous sulfur/graphene@g-C_3N_4 (S/GCN) hybrid sponge that may be used as a cathode for Li–S batteries with improved electrochemical characteristics. The outcomes of these combined effects are superior performances of 3D S/GCN in terms of high specific capacity, advantageous high-rate capability, and exceptional long-term cycling stability. Specifically, a low-capacity fading rate of 0.017% per cycle over 800 cycles at 0.3C and a high energy density of up to 1493 W h kg^{-1} are attained.[130] Furthermore, this one-pot method is straightforward to use. It eliminates the need for unwanted Li_2S_n catalysts, which simplifies the process of creating sulfur/carbon hybrid electrodes (Fig. 6a and b). Significantly, in another study published by Qu, Long, *et al.*, polysulfides were trapped using the 2D g-C_3N_4/graphene sheet composite (g-C_3N_4/GS) as an interlayer for a sulfur/Ketjen black carbon (S/KB) cathode. The interlayer of g-C_3N_4/GS combined with the sulfur-based cathode produced an exceptionally high reversible capacity of 1191.7 mA h g^{-1} at 0.1C after 100 cycles, which is significantly greater than the reversible capacity of the sulfur-based cathode alone (625.8 mA h g^{-1}). It also demonstrated extended cycling stability with a reversible capacity of 612.4 mA h g^{-1} at 1C after 1000 cycles (Fig. 6c and d).[131] Xiaoyu Wu *et al.* group synthesized an S@C-NC/GN/g-C_3N_4 cathode and performed electrochemical characterization at a rate of 0.5C. After 500 consecutive electrochemical cycles, the manufactured S@C-NC/GN/g-C_3N_4 cathode exhibits an outstanding cycling performance, maintaining a high reversible capacity of around 1130 mA h g^{-1} (Fig. 6e and f).[132]

2.2.3. Graphenes/MXenes for lithium–sulfur batteries. MXene is a 2D transition metal carbide or carbonitride emerging from the MAX phase. Many sulfur atoms can be loaded into the unusual structural variation of MXenes, and the addition of heteroatoms increases the chemisorption of polysulfide. Furthermore, the material's superior electrical conductivity and lithium-ion transport capacity enable its direct application as a sulfur carrier. The electrochemical performance of the LSBs can be noticeably enhanced with the MXene@S cathode. Engineered MXenes can help with material agglomeration and stacking issues, but the procedure is highly time-consuming and costly. Consequently, scientists have improved the MXene carbon composite material.[133–135] Ti_3C_2 is

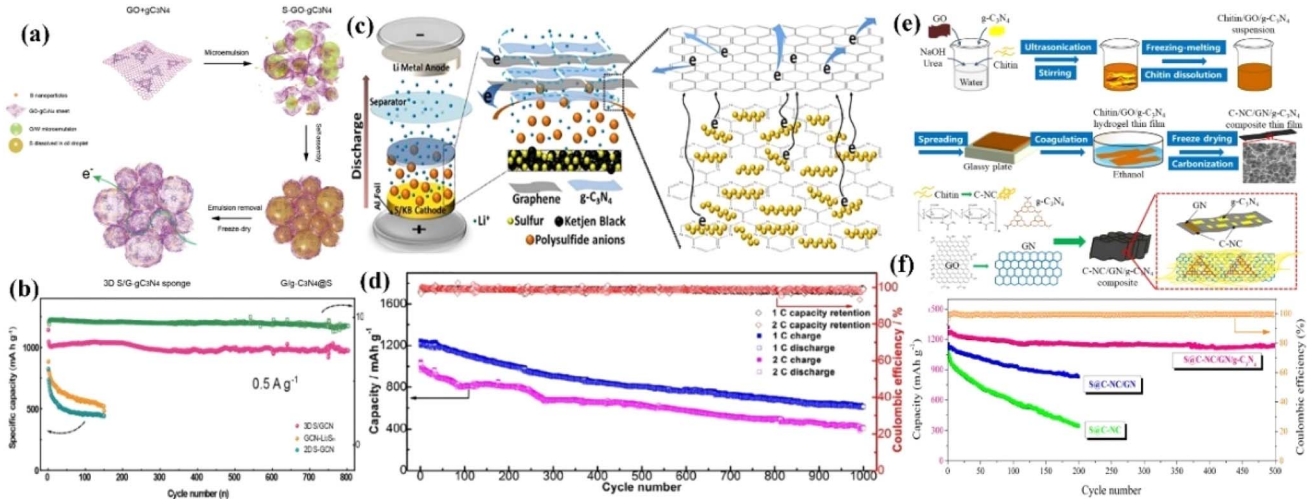

Fig. 6 (a) Schematic of the procedure for preparing S/GCN hybrid sponge. (b) Long-term cycling performance of S/GCN, GCN-Li_2S_n, and S-GCN cathodes at a low current density of 0.5 A g^{-1} (0.3C). (c) Schematic of cell configuration with a laminated structure of the g-C_3N_4/GS cathode interlayer. (d) Cycling performance and capacity retention of the S/KB@C_3N_4/GS cathode at 1 and 2C for 1000 cycles. (e) Free-standing 3D network cathode (N-doped carbon/graphene/g-C_3N_4) preparation. (f) Long cycling performance of the S@C-NC, S@C-NC/GN and S@C-NC/GN/g-C_3N_4 cathodes at 0.5C rate.[130–132]

the MXene derivative that is investigated most frequently among all of the them.[136] According to Luo Yuanzheng *et al.*, a freestanding graphene-supported N-doped $Ti_3C_2T_x$ MXene@S cathode was successfully manufactured by the co-assembly of rGO flakes onto the sulfur particles in a reduction process *via* a simple sacrificial templating approach (Fig. 7a). The battery was able to achieve a high specific capacity of 721.7 mA h g^{-1} at 0.1C and a capacity retention of 579.6 mA h g^{-1} after 300 cycles with the optimal N–$Ti_3C_2T_x$@S/G cathode despite a comparatively high loading amount of 5.2 mg cm^{-2} (Fig. 7b).[137] A functionally antagonistic Janus composite made of sulfur, graphene oxide, and $Ti_3C_2T_x$ MXene was reported by Sanghee Nam *et al.*[138] While the GO side offers significant porosity and nonelectrical conductivity, the MXene side retains mechanical qualities and

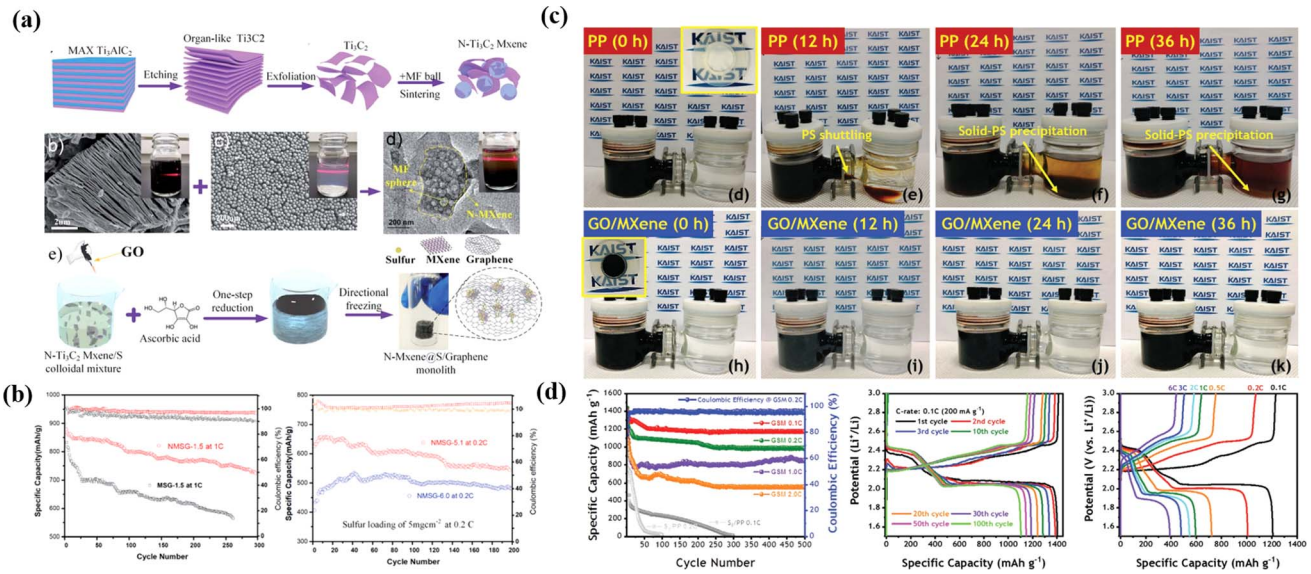

Fig. 7 (a) Schematic of the synthesis of N–$Ti_3C_2T_x$ MXene nanosheets; corresponding SEM and TEM images of $Ti_3C_2T_x$ flakes, the melamine–formaldehyde (MF) nanosphere and the $Ti_3C_2T_x$-wrapped MF nanosphere and schematic of the one-step synthesis process of the freestanding NMXene@S/G composite. (b) Long-term cycling performances of the Li–S cell with NMSG at 1C for 300 cycles. (c) Optical images of the visualized lithium polysulfide diffusion test with a commercially available PP separator and a GO/MXene bilayer composite at 0, 12, 24, and 36 h, consisting of Li_2S_6 (Left), GM (Middle), and DOL/TEGDME (Right) in a H-type electrolytic cell and electrochemical measurements; long-term cycling test at 0.1, 0.2, 1.0, and 2.0C of GSM and S8/PP cell. (d) Charge–discharge profile at a C rate of 0.1C (200 mA g^{-1}) from the 1st to the 100th cycle; charge–discharge profiles at different C rates (0.1 to 6C).[137,138]

metallic-like conductivity. As a result, GO and MXenes were employed as the selective separator and current collector, respectively. The permselectivity test in a 50 mL H-type electrolytic cell with a GO/MXene bilayer composite (GM) and a commercial PP separator is shown in Fig. 7c. The color of these two cells' right chambers was assessed after 12, 24, and 36 hours. Dark brown gradually altered in the right chamber using a PP (Fig. 7c). As seen in Fig. 7c, however, in the instance of the GM, LiPSs did not diffuse to the right chamber, and the right chamber's color remained colorless. As seen in Fig. 7d, the charge–discharge tests were carried out at different current densities ranging from 0.1 to 2.0C. With a cyclic retention of around 85.1%, the specific capacity demonstrated exceptional stability at low C rates. The particular capacities at 1.0 and 2.0C were adequately maintained despite minor variations. At 0.1 and 0.2, respectively, the initial discharge capacities were 1424.52 and 1241.67 mA h g^{-1}. At different C rates of 0.2, 0.5, 1.0, 2.0, 3.0, and 6.0C, respectively, specific capacities of 1, 046.73, 731.85, 617.86, 461.3, and 422.94 mA h g^{-1} were achieved (Fig. 7d).

2.2.4. Graphenes/transition metal dichalcogenides for lithium–sulfur batteries. Transition metal dichalcogenides (TMDs) with layered structures such as graphenes are easier to exfoliate and facilitate quick ion diffusion. TMDs exhibit multiple structural phases, with the most prevalent in the octahedral (1T) and trigonal prismatic (2H) phases. Numerous new characteristics are present in these various TMD groupings. As a result, they have been extensively employed in studying different ion battery electrode materials. In recent years, TMD and TMD/graphene composite materials have brought new life to the design of LSBs for enhanced performance. He *et al.* fabricated a graphene/1T-MoS_2 heterostructure with high-efficiency electrocatalytic properties, suppressing the polysulfide shuttle, to enhance the performance of LSBs. A few layers of graphene nanosheets were sandwiched between metallic, hydrophilic 1T-MoS_2 multilayers with many active sites to form the heterostructure (Fig. 8a). While a high conductivity of 1T-MoS_2 and graphene facilitates electron transmission, the porous 3D structure and hydrophilicity aid in the electrolyte penetration and Li-ion transfer. As shown in Fig. 8b, these benefits result in the graphene/1T-MoS_2-containing LSBs having good electrochemical performance, with a reversible discharge capacity of 1181 mA h g^{-1} and a capacity retention of 96.3% after 200 cycles.[139] Similarly, $MoTe_2$@-graphene composites were prepared quickly and easily *via* microwave synthesis by Zhen Wei *et al.* and utilized as cathode host materials for LSBs to reduce polysulfide shuttling and enhance interfacial electron/ion transport. The $MoTe_2$@-graphene@carbon cloth electrode demonstrated exceptional rate performance, good cycling stability (98.7% capacity retention after 100 cycles at 0.2C), and a high initial discharge capacity of 1246 mA h g^{-1} at 0.2C for the first galvanostatic cycle (Fig. 8c).[140] A MoS_2@ carbonized melamine foam (CF)-nitrogen-doped reduced graphene oxide (NRGO) composite was fabricated by Jiayu Zhan *et al.* and used in Li–S batteries as a modified polypropylene separator layer (MoS_2@CF-NRGO/PP) (Fig. 8d). The composite preserved a three-dimensional carbon matrix structure, which improved Li^+ shuttling conditions and improved the LiPS filtration efficiency (Fig. 8e–g). Li–S batteries featuring a separator modified by MoS_2@CF-NRGO demonstrated an exceptional rate performance of 615 mA h g^{-1} at 5C, surpassing the CF-NRGO and PP configurations (Fig. 8l).

Additionally, after 200 cycles, the MoS_2@CF-NRGO modified separator exhibits a 99.6% average coulombic efficiency, demonstrating an outstanding capacity retention. After ten charge/discharge cycles at 0.5C, Li–S batteries were allowed to rest for five days to examine their self-discharge behavior. Following a five-day rest period, the MoS_2@CF-NRGO configuration's discharge capacity drops from 1015.8 to 927.9 mA h g^{-1}, with an average self-discharge value of only 8.6% (Fig. 8l). The molybdenum disulfide/graphene (MoS_2/G) interlayer was constructed by Mingang Zhang and his team using a straightforward coating technique, and it was utilized in an LSB separator.[142] The color change of the mixed solution can be used to directly compare and evaluate the polysulfide adsorption capacity of composites (Fig. 8m). At 0.1C, the CNT/S@MoS_2/G cathode has an initial discharge capacity of 1537.2 mA h g^{-1}. At 0.5C, the CNT/S@MoS_2/G cathode has a discharge capacity of 984.9 mA h g^{-1} (Fig. 8n). With an ultralow capacity decay of 0.061% every cycle, the capacity drops to 713.8 mA h g^{-1} after 450 cycles. The CNT/S@MoS_2/G cathode delivered excellent rate capability. The MoS_2/G interlayer, which sits between the cathode and the separator, is thought to have more excellent cycling stability because it confines polysulfide to the cathode and lessens the shuttle effect.

2.2.5. Graphenes/transition metal oxides for lithium–sulfur batteries. Metal oxide-decorated graphenes both reduce the shuttle effect that polysulfides cause and improve their chemical adsorption, because of their strong surface polarity. As a result, research on graphene and metal oxide complex composites has been extensive. A double-shelled TiO_2–graphene heterostructure (H–TiO_2/rGO) with a high degree of exposure on the active plane and a lot of oxygen vacancies has been described by Yanqi Feng *et al.* as an enhanced host material for LSBs.[143] The electrode (S–TiO_2/rGO-1) combines the beneficial properties of strong anchoring and catalysing LiPSs to provide a product with excellent rate performance, a long lifespan (1000 cycles at 1C, 0.023% capacity loss per cycle), and high coulombic efficiency (Fig. 9a). The polysulfide shuttle in the LSBs was regulated by the thin TiO_2/graphene interlayer, as demonstrated by Zhubing Xiao *et al.* (Fig. 9b).[144] It was discovered that the porous carbon nanotube (PCNT)–S cathode could provide a reversible specific capacity of $\approx$1040 mA h g^{-1} over 300 cycles at 0.5C thanks to the application of the graphene/TiO_2 sheet as an interlayer (Fig. 9c). Porous graphenes provided an extra electrically conducting network and physically confined S and PS in this well-thought-out design. As an added benefit, TiO_2 in the graphene/TiO_2 barrier film further chemically suppressed PS's dissolution and lessened the undesired shuttle effect. Youlong Xu group reported that ferric oxide nanoparticles on an N, S co-doped graphene (Fe_3O_4–N, S/rGO) sheet structure may have a major impact on the development of Li–S batteries with high energy density and extended cycling life by

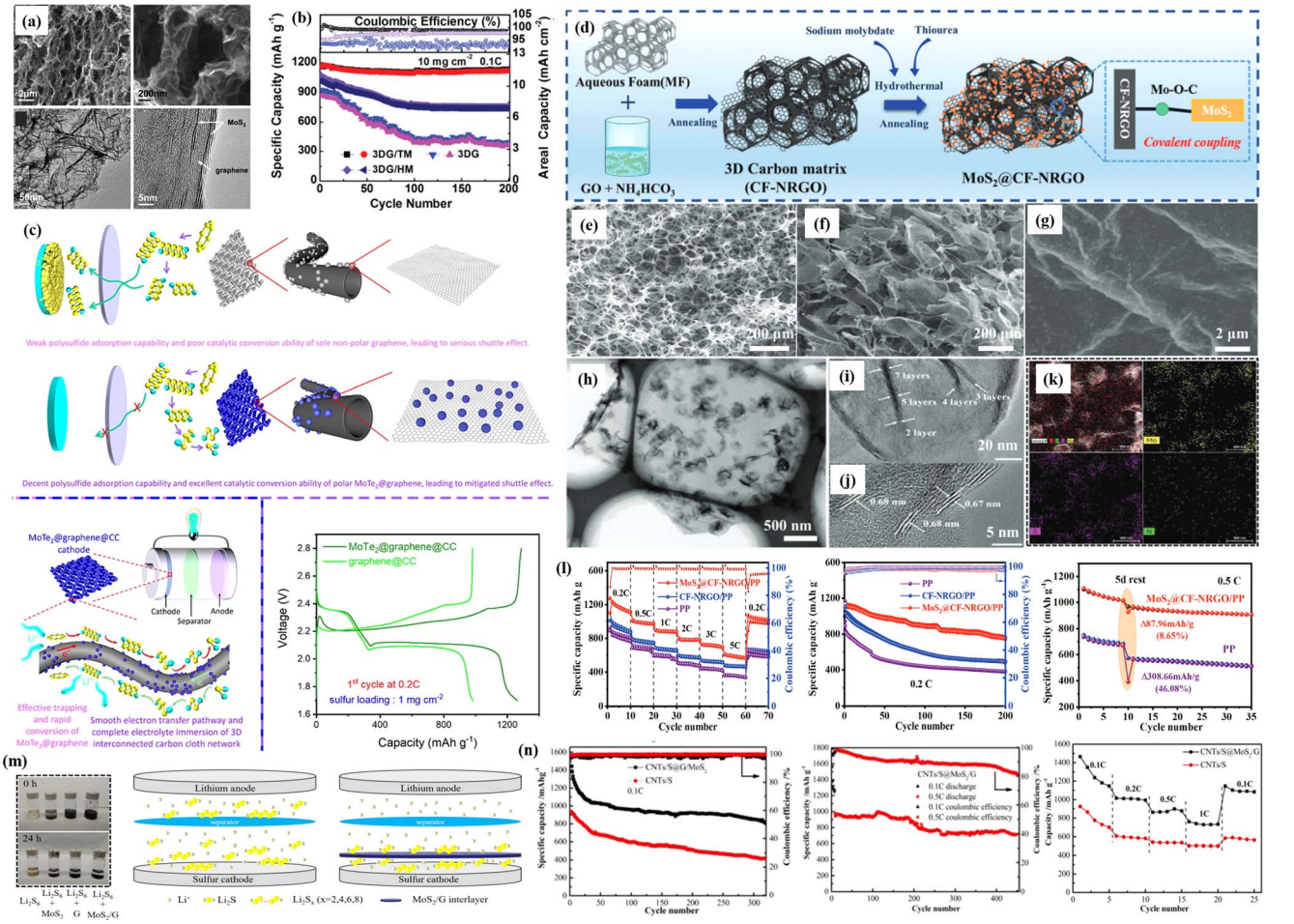

Fig. 8 (a) SEM images of 1T MoS_2 on the graphene aerogel ((three-dimensional graphene) 3DG/1T MoS_2 (TM)). (b) Cycling stability of electrocatalytically active 3DG, 3DG/1H MoS_2 (HM), and 3DG/TM as working electrodes *vs.* Li/Li^+ with a catholyte consisting of 1 M Li_2S_6 at 0.1C rate.[139] (c) Polysulfide conversion ability of polar $MoTe_2$@graphene composite as a cathode material for LSBs.[140] (d) Schematic of the preparation stages of MoS_2@CF-NRGO. SEM images of (e) carbonized MF and (f and g) MoS_2@CF-NRGO. (h) TEM and (i and j) HR-TEM images of MoS_2@CF-NRGO. (k) EDS mapping images of MoS_2@CF-NRGO and the corresponding images of Mo, S, and N. (l) Rate capacity and cycling capabilities at 0.2C of a cell with the MoS_2@CF-NRGO/PP separator, CF-NRGO/PP, and PP separators and cycling performance at 0.5C before and after rest of the MoS_2@CF-NRGO/PP and PP separators,[141] (m) digital photographs of MoS_2 and MoS_2/G composites in a Li_2S_6 solution for 0 and 24 h; schematic of the lithium–sulfur battery without and with the MoS_2/G interlayer. (n) Cycling performance and coulombic efficiency of the carbon nanotube (CNT)/S@MoS_2/G and CNT/S cathodes at 0.1C, cycling performance and coulombic efficiency of the CNT/S@ MoS_2/G at 0.5C and rate capability.[142]

controlling LiPSs and improving the conversion kinetics.[145] Using a straightforward microwave hydrothermal process (Fig. 9d), ferric oxide nanoparticles on an N, S co-doped graphene (Fe_3O_4–N, S/rGO) sheet structure were fabricated and used as the cathode for LSBs. In the end, the built Fe_3O_4–N, S/rGO–S batteries provide consistent long-term cycle life and high-rate capability. The Fe_3O_4–N, S/rGO–S electrode continues to provide a high discharge specific capacity of 1004 mA h g^{-1} even after 200 cycles at 0.5C (Fig. 9e).

2.3 Graphene-based 2D materials for lithium–O_2 and lithium–CO_2 batteries

Rechargeable Li–O_2 and Li–CO_2 batteries, which offer a higher theoretical energy density than that of Li-ion batteries, have recently attracted a lot of attention.[146,147] Li–O_2 batteries have been developed to fulfil the increased demand for electric energy in today's world. The formation of a lithium peroxide (Li_2O_2) product, which has a substantially higher energy storage capacity than that of other energy storage systems, is responsible for the high energy density of Li–O_2 batteries.[148] The high band gap of solid Li_2O_2, which is probably covering the catalytic sites, makes charge transfer necessary for the breakdown of Li_2O_2 during the charge process difficult.[149] This results in a slow charging process that raises the potentials needed for Li_2O_2 breakdown, which lowers the battery's energy efficiency and increases the danger of electrolyte degradation.[150,151] Furthermore, the size and shape of the Li_2O_2 product can affect the charge potential. Developing Li–O_2 batteries requires improving the materials used in each component of the battery in order to address knotting problems. Two-dimensional materials have recently attracted attention due to their

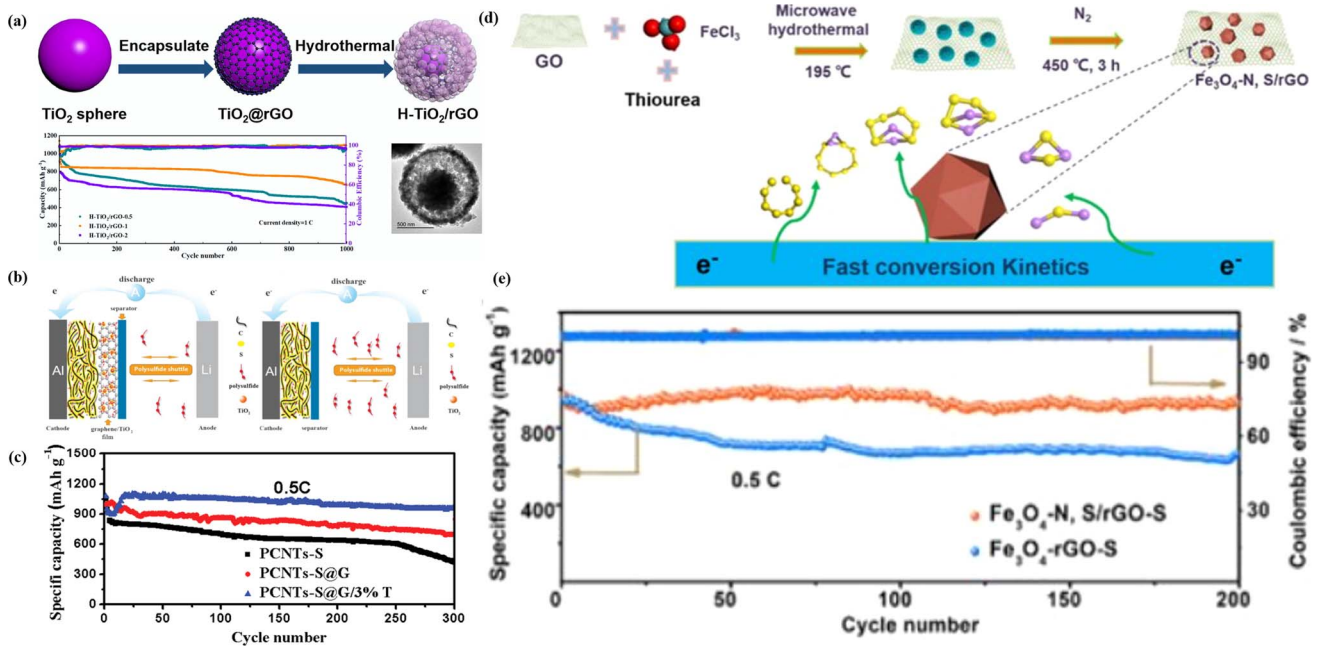

Fig. 9 (a) Schematic of the formation and long-term cycling performances at a current density of 1C of H–TiO_2/rGO-1.[143] (b) Schematic of the electrode configuration for the Li–S battery with a graphene/TiO_2 coating film and conventional Li–S battery. (c) Cycling stability of PCNTs–S, PCNTs–S@G, and PCNTs–S@G/3% TiO_2 cathodes at 0.5C, and a current density of 0.86 mA cm^{-2}.[144] (d) Schematic of the synthesis process of the Fe_3O_4–N, S/rGO composite. (e) Cycling performance of the Fe_3O_4–N, S/rGO–S and Fe_3O_4-rGO–S electrode at 0.5C after 200 cycles.[145]

potential to improve the Li–O_2 battery performance. This is because of their distinct designs, which have the potential to effectively address a number of issues related to the electrode materials (cathode and anode), solid-state electrolyte, and separator in Li–O_2 batteries.[152–155] A unique type of MnO_2@rGO nanocomposite material was described by Lihua Zhu *et al.*; it is very effective for Li–O_2 batteries and consists of extremely few nano-sized MnO_2 grains on the surface of rGO (Fig. 10a). In Li–O_2 batteries, MnO_2@rGO composites were used as cathode catalysts with a cut-off capacity of 1000 mA h g^{-1} and a current density of 200 mA g^{-1} (Fig. 10b).[156] Over 60 cycles, batteries based on MnO_2@rGO demonstrated a consistent discharge capacity. Strong synergistic effects between the rGO framework and the nano-sized MnO_2 particles on its surface are responsible for the exceptional performance. Functionalized graphenes with an optimal bimodal porous structure were produced by Jie Xiao *et al.* for Li–O_2 battery operation (Fig. 10c). A novel air electrode that uses an uncommon hierarchical configuration of functionalized graphene sheets produces the highest capacity of 15 000 mA h g^{-1} at around 2.7 V.[85] Yuejiao Li and colleagues described the facet engineering of an ultrathin, two-dimensional Mn_3O_4 nanosheet on graphene (Mn_3O_4 NS/G) with the dominating (101) crystal planes. The goal of this catalyst is to generate durable, effective oxygen for high-performance Li–O_2 batteries that exhibit ultrahigh capacity and long-term stability, offering a lower charge overpotential (Fig. 10d).[157]

Similar to Li–O_2 batteries, the Li–CO_2 battery is another advanced technology because of its high theoretical energy density of 1876 W h kg^{-1}. Li–CO_2 batteries offer a novel method for capturing CO_2 and advancing the development of electrochemical energy storage systems of the next generation by using CO_2 as the active material at the cathode. Rechargeable Li–CO_2 batteries store energy by breaking down the discharge products when exposed to external electricity during the charging process. During discharge, this process produces electricity *via* a redox reaction between the Li anode and the CO_2 cathode, namely Li_2CO_3.[159–161] Zhang Zhang *et al.* reported the first introduced graphene as a cathode material to improve the performance of Li–CO_2 batteries.[162] Wei Yu *et al.* synthesized N, O-diatomic graphene carbon aerogels by a straightforward, one-step thermal approach and used it as a cathode Li–CO_2 battery. The resulting Li–CO_2 batteries demonstrated an impressive cycling stability of more than 1500 h at 20 μA cm^{-2} and a significantly improved initial energy efficiency of about 78.46%.[160] MXene-based materials have been used as the cathode in Li–CO_2 batteries because of their superior interlayer ion transport channels, strong electrical conductivity, and chemical composition's tunability. Wentian Zhao prepared porous TVGA *via* a hydrothermal reaction and used it as a cathode in Li–CO_2 batteries (Fig. 10e). The TVGA cathode has flexible nature, and hence, a flexible Li–CO_2 battery was fabricated and used in different bending angles. Light-emitting diodes (LEDs) can be steadily lit by a Li–CO_2 battery without any adjustments (Fig. 10f). Fig. 10g compares the cycling performance of Li–CO_2 batteries with different cathodes. At a current density of 200 mA g^{-1}, TVGA displays a comparatively low overpotential of 1.5 V.[158] The battery has a 91 times stable cycling capacity at 200 mA g^{-1}, with an over potential of 1.5 V for both charging and discharging. These exceptional

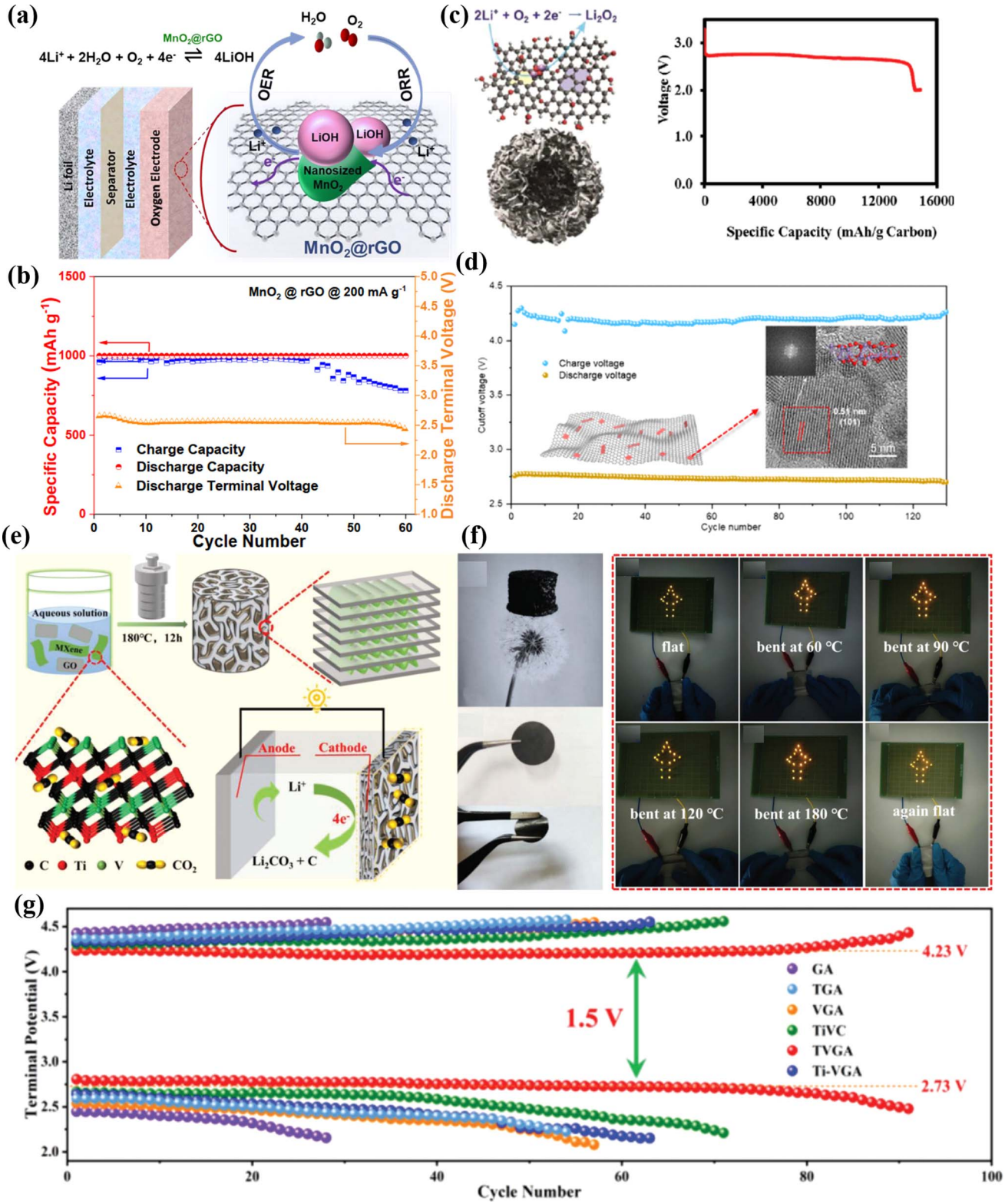

Fig. 10 (a) Schematic of the structure catalyzed by MnO_2@rGO for the Li–O_2 battery. (b) Discharge/charge capacity of MnO_2@rGO for the Li–O_2 battery at a current density of 200 mA g^{-1}. (c) An optimal bimodal porous structure on a functionalized graphene sheet (FGS) and the discharge curve of a Li–O_2 cell using the FGS. (d) Two-dimensional Mn_3O_4 nanosheets on graphene with charge/discharge voltages. (e) Li–CO_2 battery's schematic, optical picture and flexible optical picture of the TiVC/rGO aerogel (TVGA) cathode sheet. (f) LEDs with the flexible Li–CO_2 battery. (g) Variation in the terminal polarization of Li–CO_2 batteries with different cathodes at a current density of 200 mA h g^{-1}.[85,156–158]

electrochemical performances are due to the special synergistic interaction between Ti and V in TiVC, which improves the reversible formation and breakdown of the discharge product Li_2CO_3 by enhancing the interfacial chemical bonding ability, realizing the full exposure of active sites and promoting the catalytic interfacial structural reorganization. In the meantime, the aerogel's rich pore structure helps lower the mass and charge transfer resistance by promoting the diffusion of CO_2 and electrolytes in addition to helping to enhance ion transport.

3. Lithium metal anode modification with graphenes

Since lithium metal has the lowest working potential (−3.04 *vs.* conventional hydrogen electrode) and the largest specific capacity (3860 mA h g^{-1}), it has been considered the best option for lithium-ion battery anodes. The lithium metal anode, a crucial component of the next generation of high-energy density lithium metal batteries (LMBs), has gained significant interest from both industry and academics. However, because of its innate propensity to generate dendrites during cycling, the lower cycling stability and safety concerns have long hindered the adoption of lithium metal anodes. The excessive parasitic interactions between the Li metal dendritic growth and the liquid electrolyte result in the irreversible consumption of both the electrolyte and active lithium. Consequently, the rapid capacity decline and catastrophic cell failure of LMBs are explained by the production of Li dendrites. Several methods have been devised to enhance the lithium metal anode's cycling stability and controlling the Li dendrites.[163–169] According to David Mitlin and colleagues, a significant degree of structural and chemical imperfection in graphene leads to unstable SEI formation. This is associated with the rapid decline of coulombic efficiency and the production of filament-like Li dendrites, as well as the consumption of the fluoroethylene carbonate (FEC) additive in the carbonate electrolyte.[164] Pinxian Jiang *et al.* described the graphene hybrid architecture as a lithiophilic host for a high-performance Li metal anode. They utilized it in the LMB to synthesize a nanosheet/graphene heterostructure composite *via* a polymer-assisted sonochemical process. The Li metal anode that results from the graphene hybrid architectural scaffold shows stable cycling over 200 cycles at 0.5 mA cm^{-2} (2 mA h) and provides a high energy density of 402 W h kg^{-1}.[170]

4. Hydrogen production and storage

4.1 Sustainable green hydrogen production approaches

Hydrogen (H_2) is recognized as an efficient energy carrier as it is an eco-friendly, non-toxic, renewable, and less costly energy source. Currently, H_2 is generated from renewable and non-renewable sources, where only 95% of H_2 is from non-renewable fossil fuels, and 5% is from renewable sources such as solar and wind.[41] The H_2 production approaches dependent on non-renewable resources are associated with CO_2 emissions, are expensive and energy-intensive, and involve harsh operating conditions.[171] Thus, researchers are exploring approaches to generate sustainable, less costly, and zero carbon-emitting H_2 energy.[172] In terms of renewable energy, the role of abundantly existing solar energy is significant, and two approaches for H_2 production can be employed, namely, (1) photocatalytic and (2) photoelectrochemical. Photocatalytic H_2 production by water splitting using semiconductor catalysts is a widely researched, less costly, eco-friendly, and effective approach for green H_2 generation.[173,174] Moreover, PEC water splitting for H_2 production is another approach that uses solar-irradiated photoelectrodes and an external bias voltage to suppress charge recombination, leading to excellent overall performance.[175]

4.1.1. Mechanism of photocatalytic and photoelectrochemical H_2 production. Generally, an efficient photocatalytic setup needs a catalyst capable of absorbing visible irradiation as a major part of sunlight constitutes irradiation within the visible range, a suitable photoreactor, and a sacrificial agent (Table 1).[191] Moreover, an effective interaction between all the components of the photocatalytic setup is needed for significant performance improvement.[192] Overall, water splitting into H_2 and O_2 is not favorable in terms of thermodynamics under normal temperature and pressure conditions because of the existence of strong bonds in H_2O and its low power to ionize. Therefore, at room temperature, the entire process needs 237 kJ mol^{-1}, *i.e.*, 2.46 eV per H_2O molecule of Gibbs free energy (ΔG).[193] The photocatalytic H_2 generation process initiates after the semiconductor catalyst absorbs the solar irradiation, having a wavelength greater than or equal to the semiconductor band gap to generate electron–hole pairs followed by the separation of charges where electrons jump to the conduction band (CB) of the semiconductor and holes are left in the valence band (VB). Then, a redox reaction occurs, where the electrons play a role in the reduction of H^+ to H_2, and the holes are responsible for oxidizing H_2O into O_2.[194] Eqn (1)–(3) describe the steps involved in overall photocatalytic H_2 generation. Moreover, for the photocatalytic process, the energy level of the semiconductor CB should be at a potential less than 0 V ($E(H^+/H_2)$) for the reduction process, and the VB energy level should be at a higher potential than 1.23 V ($E(O_2/H_2O)$) to conduct oxidation reactions.[195,196] Fig. 11a illustrates the photocatalytic H_2 generation mechanism over photocatalysts.

$$2H^+ + 2e^- \rightarrow H_2 \quad (1)$$

$$2H_2O + 4h^+ \rightarrow O_2 + 4H^+ \quad (2)$$

$$2H_2O + 2O_2 \rightarrow 2H^+ \quad (3)$$

The PEC H_2 production utilizes a PEC cell comprising two or three electrodes acting as semiconductors for photoelectrodes submerged in an aqueous electrolyte, with the electrodes separated by a membrane.[195] Out of the electrodes used, one or two electrodes should have the potential to be activated under irradiation. Normally, the PEC comprises three electrodes for water splitting: a photoanode and a cathode act as active

Table 1 Summary of the recent 2D graphene-based nanocomposites as photocatalysts for photocatalytic H_2 production together with the yield of H_2 and parameters, including loading of catalyst, source of light, and sacrificial agent

Photocatalyst	Catalyst loading (mg)	Light source	Sacrificial agent	H_2 production ($\mu mol\ g^{-1}\ h^{-1}$)	Ref.
TiO_2/rGO/MoS_2	50	3 W 4 LEDs (λ 365 nm)	10 vol% methyl alcohol	880	176
2D CN@graphene@CN	10	300 W Xe lamp with 420 nm cut-off filter	10 vol% TEOA	5580	177
Few-layer graphene (FLG)/g-C_3N_4	0.15 g L^{-1}	4 LEDs of 880 W m^{-2} each (420 nm)	10% v/v ethylenediaminetetraacetic acid (EDTA) and 3 wt% Pt	1274	178
0D-2D-2D CdSe QD/B-rGO/O-gC_3N_4	30	Xe arc lamp (λ > 400 nm)	Triethanolamine (TEOA)	1435	179
Ni_2P/rGO/g-C_3N_4	10	300 W Xe lamp (λ > 420 nm)	10 vol% TEOA	2921	180
CdS@h-BN/rGO	10	Simulated solar light	10 vol% triethanolamine (TEA)	6465.33	181
P.RGO/MoS_2	2	400 W Xe lamp	20% (v/v) TEOA and 1 mL eosin Y	11 230	182
2D/2D MoS_2/g-C_3N_4-Au	200	300 W Xe lamp 420 nm cutoff filter	20 mL methanol	1100	183
Molybdenum sulfoselenide (MoSSe)@RGO	—	400 W Xe lamp ($\lambda \geq$ 420 nm)	Eosin Y and TEOA	5016	184
GQD/TpPa-1-COF	20	300 W Xe lamp	0.1 mol per L ascorbic acid	487	185
2D/2D Cu-tetrahydroxyquinone MOF (CuTHQ)/N-doped graphene (NG)	20	150 W Xe lamp	Methanol (MeOH)	164	186
Co-BDC MOF/GO	—	150 W halogen lamp	0.2 M TEOA and EY photosensitizer	14.5	187
2D/2D PRGO/CdS-diethylenetriamine (DETA)	50	0.35 M Na_2S, 0.25 M Na_2SO_3 and Pt cocatalyst	300 W Xe lamp with 400 nm cut-off filter	10 500	188
Cu_2O/RGO/$BiVO_4$	50	30 mL tetracycline	300 W Xe arc lamp (λ > 420 nm)	5.95	189
rGO-coupled C_3N_4/C_3N_5	50	10 vol% TEOA	300 W Xe lamp ($\lambda \geq$ 400 nm)	6380	190

electrodes, while Ag/AgCl acts as a reference electrode. As shown in Fig. 11b, n-type semiconductors have excess electrons and thus are used as photoanodes. Conversely, p-type semiconductors function as photocathodes due to their excess electron–hole pairs. Electrons are excited and move from the VB to the CB when the photoanode is exposed to light with an energy higher than its energy bandgap, followed by the movement of electrons toward the cathode to carry out a reduction reaction, while the holes left behind are involved in the process of oxidation.[200,201] With the need for an overpotential for each half-reaction, electrode resistance, loss from charge carriers' recombination, and potential decline at contacts, the energy required for PEC water splitting in practical systems can approach 2 V. To compensate for these losses and supply the energy needed for water splitting, an external bias is frequently used.[202] Fig. 11c illustrates the steps involved in the PEC water splitting mechanism for H_2 generation.

4.1.2. Overview of photocatalysts and 2D graphenes for green H_2 production. The overall water splitting involving the generation of H_2 and O_2 is an uphill process, requiring 1.23 eV energy. Therefore, the major prerequisite of a suitable catalyst is the band gap, which should be higher than 1.23 eV. Since 1972, after the exploration of water splitting by Honda and Fujishima, where a photoanode comprising TiO_2 and Pt cathode was used,[203] various catalysts including nitrides, oxides, sulfides, and carbides have been extensively explored for H_2 production *via* water splitting. The efficiency of all the explored catalysts is dependent on the solar light absorption ability, generation of charge carriers, separation of charge carriers, redox ability, more exposed surface area and stability. Moreover, the non-toxic nature and low cost are also the requirements for selecting a suitable catalyst for H_2 generation.[197,204–206]

Earlier, various semiconductor materials such as TiO_2,[207] $BiVO_4$,[208] WO_3,[209] perovskites,[210] g-C_3N_4,[211] LDHs,[212] ZrO_2,[213] and CdS[214] as photocatalysts have been researched for photocatalytic H_2 generation; however, they show poor efficiency towards photocatalytic H_2 generation mainly due to lower stability, wide band gap, and charge carrier recombination, whereas the photocatalysts having a narrow band gap suffer from a lower efficiency based on their surface area.[215] The utilization of metal-based photocatalysts is also explored extensively; however, metals are toxic and at the same time expensive.[216] In this regard, 2D materials as semiconductors for photocatalysis have attracted substantial attention as they offer excellent optical characteristics, good mechanical features, large surface area and less distance for the movement of electron–hole pairs to the solid–water interface.[217] Particularly, the heterojunction formation of 2D graphenes having a honeycomb structure with other semiconductor photocatalysts is considered to improve the overall photocatalytic H_2 production efficiency.[218] This is associated with the existence of an exceptional sp^2 hybrid C framework, making it highly conductive for thermal energy, *i.e.*, about 500 W m^{-1} K^{-1} and depicts an exceptional charge migration under ambient temperature condition, *i.e.*, about 200 000 cm^2 V^{-1} s^{-1}.[219] Besides, it shows a zero band gap and an enhanced surface area of about 2600 m^2 g^{-1}. Graphene-based

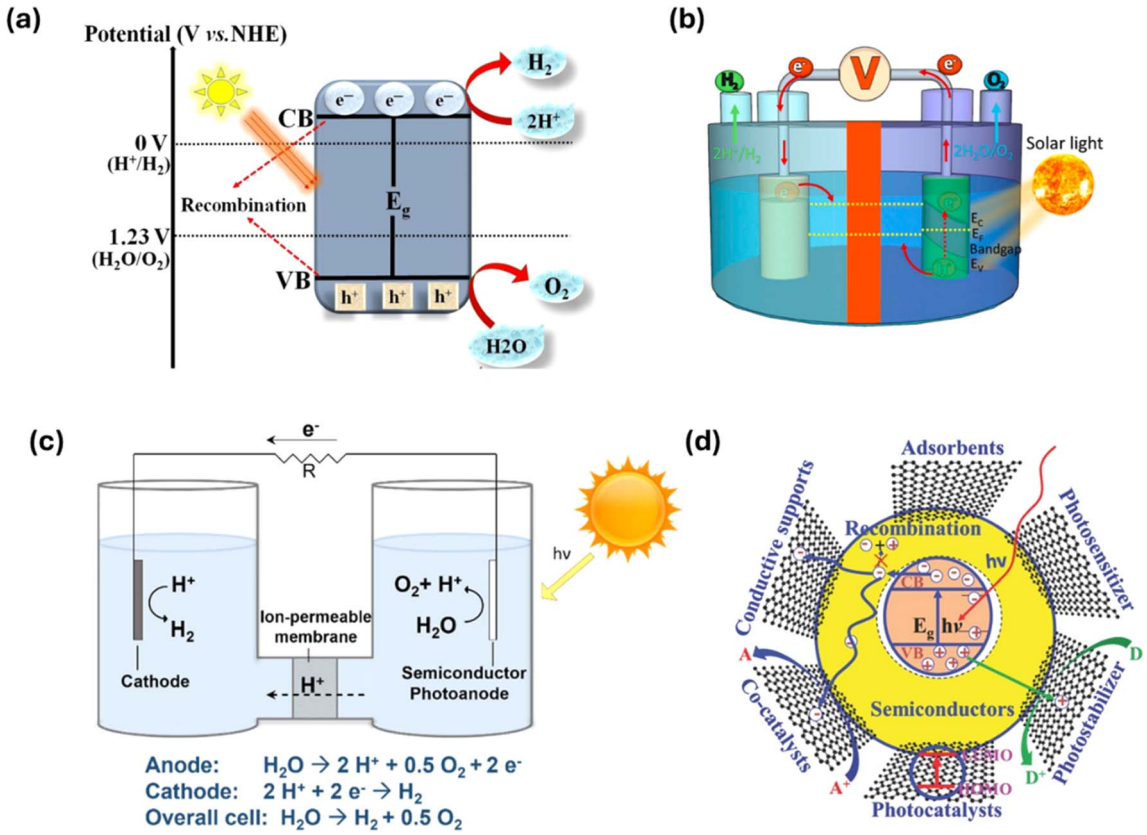

Fig. 11 (a) Illustrative overview of the general photocatalytic H_2 generation mechanism. (b) Representation of photoanodes and cathode semiconductors for PEC H_2 generation. (c) Mechanism of PEC water splitting for H_2 generation. (d) Characteristics of graphene for photocatalytic and PEC H_2 production.[197–199]

photocatalysts depict improved transfer and separation of electron–hole pairs.[220] Numerous published works used rGO as one of the standard semiconductor materials for improving the performance. RGO enhances the photocatalytic activity of these composites by facilitating the separation of electron–hole pairs across the catalyst/RGO contact. The photocatalytic H_2 production of the nanocomposites is largely dependent on the type of interface and defects present in the produced rGO.[221] rGO is unique as it possesses a variety of qualities that promote photocatalytic H_2 production efficiency. These properties include increased light utilization, charge carrier separation, intrinsic catalytic activity, and stability under operating conditions. While other photocatalysts could need co-catalysts or extra modifications to operate on par, their appropriateness varies depending on the demands of the given application and optimization techniques.[222] The efficient photocatalytic H_2 generation by graphene-based photocatalyst materials is due to the following mechanisms (Fig. 11d): (1) reduction of charge carrier recombination, (2) presence of catalytic active sites for reactions, (3) improved adsorption, (4) tunable band gap, and (5) potential to act as photosensitizers and cocatalysts.[59] Graphene derivatives including graphene oxide (GO) and reduced graphene oxide (rGO) contain epoxy, hydroxyl, and carboxyl surface groups having O_2, acting as catalytic reaction sites and also as supports for the uniform dispersion of metallic ions for nucleation and growth.[223] The dark colors of both GO and rGO lead to better absorption of light, expanding the absorption from the UV to the visible region.[224]

In the case of PEC H_2 production, photoelectrodes must possess the following features: (1) efficient absorption in the visible region, (2) appropriate band gap and positions for band edge to carry out redox reactions, and (3) stable nature in solutions of different pH values.[49] PEC H_2 production has been extensively studied for photocatalytic semiconductors such as TiO_2, MoS_2, WO_3, ZnO, α-Fe_2O_3, $BiVO_4$, Cu_2O, CdS, and Cu/Zn/W sulfide; however, certain challenges persist, leading to their poor PEC activity. For instance, TiO_2,[225] WO_3,[226] and ZnO[227] constitute wide band gaps and charge recombination, whereas α-Fe_2O_3 suffers from the demerits of short lifetime of charges, electron–hole pair recombination and less conductivity,[228] $BiVO_4$ also shows charge recombination[229] while Cu-based electrodes face the issue of photo corrosion, leading to less efficient PEC performance.[230] Lately, C-based materials such as graphene derivatives and rGO were studied to act as supports for developing different photoanodes due to their high surface area, excellent conductivity, charge movement, and stability.[231] Along with other semiconductor materials, they are known to show improved overall migration of charges, improve the photocurrent response and inhibit the process of photo corrosion.[232]

Moreover, regarding heterojunction formation, 2D/2D heterostructures are known to depict excellent interface, leading to an improved surface area and less resistant electron transfer. Compared to the conventional interface, the 2D/2D interface provides a faster transport of charges which reduced their recombination.[233] Moreover, 2D/2D heterojunctions help in tuning the band edges for efficient redox reactions.[234] The heterojunction also leads to a stable heterostructure, less agglomeration and less photo-corrosion phenomena.[235]

4.1.3. Graphene-based 2D nanocomposites for photocatalytic hydrogen production. Regarding the utilization of graphene-based nanocomposites, due to the efficient electro movement in GO, MoS_2 were grown onto rGO followed by TiO_2 coupling. The H_2 production under UV light was 88 folds more than the H_2 production from pure TiO_2 because of the synergistic effect based on the ability of rGO towards efficient electron migration and MoS_2 acting as active sites.[176] The Ti_3C_2/TiO_2/rGO nanocomposite was studied for H_2 generation and the nanocomposite generated 808.11 μmol g^{-1} h^{-1} of H_2 within the 1st h, associated with the presence of the rutile phase of TiO_2 and rGO, which offered the pathway for the migration of electrons and minimized the recombination of charges.[236] A 2D carbon nitride (CN)@graphene@CN loaded with Pt was explored for photocatalytic H_2 generation, where under light irradiation, the electrons from the CB of CN were transferred to the graphene. The graphene aided in trapping the electrons and at the same time helped in their movement to the edges for their reaction with protons (Fig. 12a). The efficient activity was concluded to be dependent on the enhanced visible light absorption, excellent transfer of electrons across the interface, spatially divided redox active sites and the presence of excess active sites.[177] In another study, 2 wt% few-layer graphene (FLG)/graphitic carbon nitride (GCN) depicted 4-times 1274 μmol g^{-1} h^{-1} of H_2 under visible light, as shown in Fig. 12b and c along with an excellent stability over 4 consecutive cycles. As shown in Fig. 12d, electron–hole pairs were generated in CN, while the layered and 2D structure of CN aided in electron transfer from CN to FLG. FLG constitutes good electric conductivity, thus providing pathways for the movement of electrons, inhibiting electron–hole pair recombination. Moreover, the greater work function of the Pt metal enabled the transfer of electrons from FLG to Pt, for H_2 generation, while holes in GCN were quenched by the sacrificial agent.[178] Ni_2P/rGO/g-C_3N_4 was explored for efficient visible light-induced H_2 production and stability, which was associated with the active sites provided by Ni_2P and the synergistic effect of rGO towards the migration of electrons, leading to less charge recombination.[180] As shown in Fig. 12e, a solution-phase electrostatic assembly of polymer-functionalized rGO and boron carbon nitride (BCN) having positive and negative charges, respectively was used to synthesize polymer rGO (P.rGO) and polymer BCN (P.BCN). The 2D nanocomposite P.rGO/MoS_2 generated the highest yield of H_2 based on the presence of active sites for the reaction and improved the migration of charges within the layered structure.[182] In a current study, graphene quantum dots (GQDs)/TpPa-1-COF were studied for photocatalytic H_2 production, where the GQDs acted as photosensitizers for improving the light absorption and acted as a trap for electrons, leading to reduced recombination of electron–hole pairs. Moreover, the movement of electrons was aided due to the presence of an ohmic interaction among the covalent organic frameworks (COF) and GQDs.[185] In another work, the need for a noble metal as a cocatalyst was diminished while using 2D/2D Cu-tetrahydroxyquinone MOF (CuTHQ)/N-doped graphene (NG) nanocomposites for H_2 production. This was linked to the efficient migration of electrons between both photocatalysts, leading to less charge recombination. Therefore, the 2D/2D heterojunction helped in an increased yield of H_2 but at the same time played a vital role in separating electron–hole pairs, leading to noble metal-free photocatalytic H_2 generation.[186] Another noble metal-free photocatalytic H_2 generation was achieved by the fabrication of eosin Y (EY) dye-sensitized earth-abundant cobalt (Co-BDC) MOF with the addition of GO, where GO played a vital role as compared to EY in improving the H_2 generation under visible light irradiation. As shown in Fig. 12f, the irradiation is absorbed by the EY dye for the generation of singlet excited state, followed by quenching by TEOA or formation of ^{3}EY* and leading to quenching by amines for the generation of radical EY anions. Then, an electron migration from EY to GO occurs followed by migration to the MOF, which was considered the main reason for efficient H_2 generation.[187]

In conclusion, GO-based photocatalytic nanocomposites showed efficient and economic H_2 generation based on the improved surface area, migration of charges, separation of charges and provision of active sites. The incorporation of GO as a cocatalyst was explored to have the potential of replacing noble metals for photocatalytic H_2 generation. The 2D/2D GO/g-C_3N_4 heterojunction incorporated into other semiconductors was extensively studied for H_2 generation based on its simple fabrication, non-toxicity, efficient charge separation and transfer and active sites.

4.1.4. Graphene-based 2D nanocomposites for photoelectrochemical hydrogen production. LDHs are known to have a layered structure and good physio-chemical characteristics, but they are less conductive, have slow kinetics and are not stable in acids. The PEC H_2 production ability of the LDH was improved by forming 2D LDH@graphene and g-C_3N_4 heterojunction with MoS_2 as a co-catalyst (Fig. 12g). The heterojunction showed good production and stability for PEC H_2 production and also effectively separated the charges.[237] In another work, the MoS_2 was fabricated onto graphenes with Ag, which showed a photoconversion of 2.2% at −0.58 V for PEC water splitting. This is due to the plasmonic effect of Ag, leading to improved visible light absorption, and due to the heterojunction, which promoted charge segregation and migration. The Fermi level of pure graphene was positioned among the MoS_2 CB and the ITO, leading to electron withdrawal to the cathode, as indicated by Fig. 12h.[238] MoS_2/crumpled N-doped graphene p–n nanojunction was explored for PEC H_2 generation with an overpotential of approximately 100 mV *vs.* reversible hydrogen electrode (RHE). The N doped onto graphenes acted as support for the anchorage of MoS_2 and the presence of crumpled graphenes minimized the accumulation. Overall, the heterojunction helped in electron–hole pair separation.[239] Two-

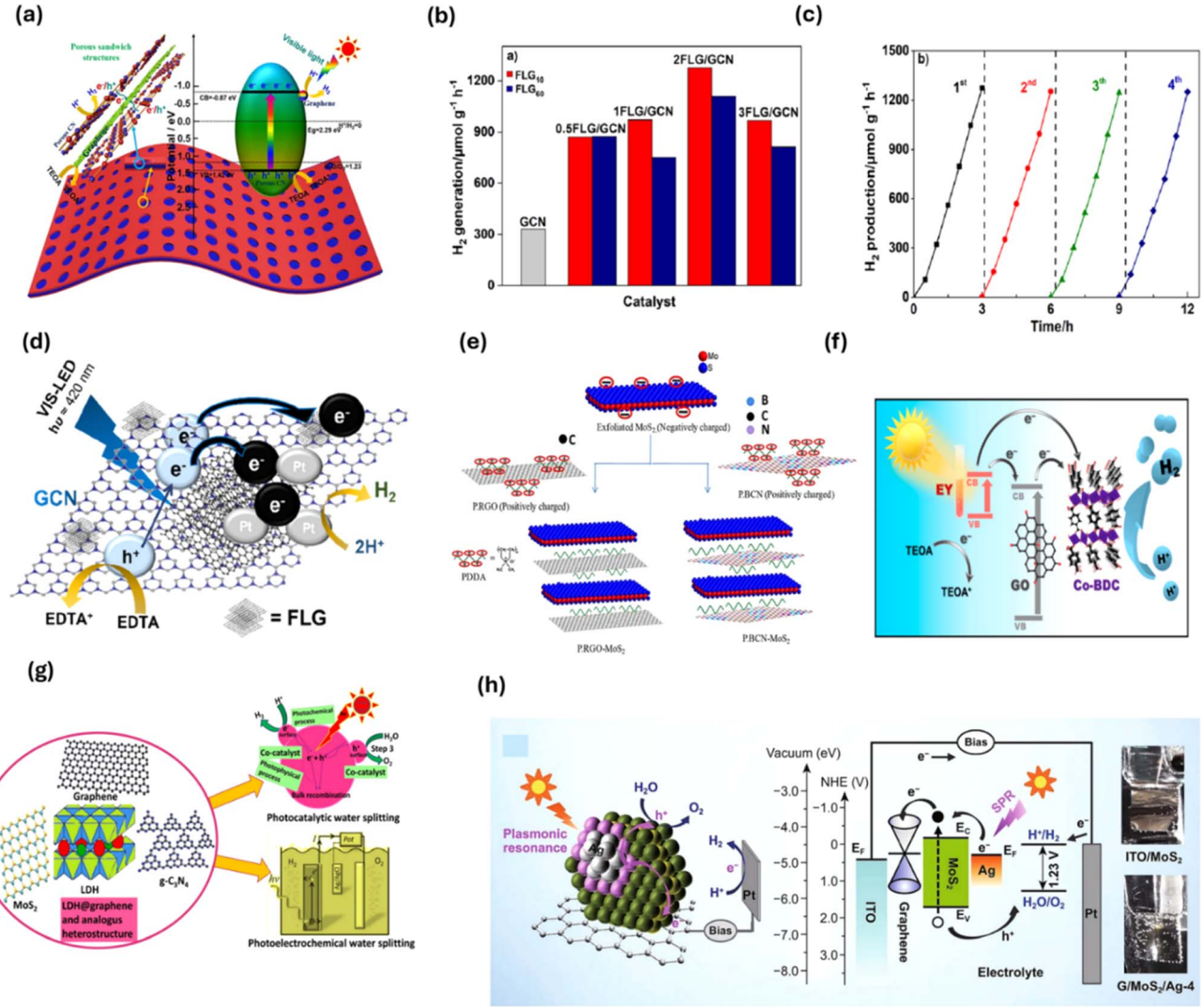

Fig. 12 (a) Illustrative overview of the charge transfer mechanism for the photocatalytic H_2 production process using 2D CN@graphene@CN loaded with Pt. (b) Rate of photocatalytic H_2 production and (c) stability over 4 consecutive cycles using FLG/GCN nanocomposites. (d) Charge transfer mechanism in the FLG/GCN nanocomposite. (e) Overview of the solution-phase electrostatic assembly to synthesize P.rGO and P.BCN. (f) Photocatalytic H_2 production mechanism in EY dye-sensitized Co-BDC MOF/GO. (g) Two-dimensional LDH@graphene and g-C_3N_4 heterojunctions for PEC H_2 generation. (h) Overview of the suitable Fermi level alignment and PEC H_2 generation in Ag-deposited MoS_2/GO.[177,178,182,187,237,238]

dimensional RGO wrapped in nanotubes of TiO_2 with decorated 2D MoS_2 was synthesized for H_2 generation, which was linked to the efficient charge transfer and the control on immobilized active sites.[240] A hybrid Ag@g-C_3N_4/r-GO nanocomposite was synthesized for PEC H_2 generation under visible irradiation. The nanocomposite showed durability, efficient activity and adaptability for PEC reaction. An apparent quantum yield of 1.69 and a rate of 954 μmol g^{-1} h^{-1} for photocatalytic H_2 generation were achieved in the presence of simulated solar light while an overpotential value of 0.484 V at a current density of 10 mA cm^{-2} was achieved in PEC H_2 generation activity.[241] In another study, a graphene/WS_2 nanocomposite was explored as a photoanode for PEC H_2 generation. The nanocomposite depicted an efficient absorption of 98% under visible irradiations. The increased visible light absorption resulted in excellent generation of electrons with improved movement of charges.[242]

In conclusion, the literature to date has shown that adding graphenes at certain interfaces can improve the PEC efficiency of photoelectrodes towards PEC H_2 generation. The high electric conductivity of graphenes, which enhances the charge carrier movement across the heterojunction components, is responsible for the significant increases in the efficiency; however, in literature for PEC H_2 production using 2D/2D graphene and its derivatives.

4.2 Hydrogen storage using graphene-based nanomaterials

Graphene-based 2D nanomaterials are found to be promising candidates for practical solid-state hydrogen storage applications due to their exceptionally large surface area (2600 m^2

Table 2 Hydrogen storage using various graphene-based nanomaterials

Material	Pressure (bar)	Temperature (K)	Hydrogen storage (wt%)	Reference
Graphene nanosheets	100	298	0.9–1.5	244 and 245
	10	77	1.2	
Hierarchical graphene	1	77	4.0	246
Graphene oxide	50	298	1.4	247
Functionalized graphene with $ClSO_3H$	2	77	1.6	248
Functionalized graphene with oleum	2	77	1.4	
Functionalized graphene with Pt nanoparticles	57	303	0.15	249
Functionalized graphene with Pd nanoparticles	40	298	0.81	250
N-doped graphene	90	298	1.5	251
Li-decorated N-doped penta graphene	—	—	7.88	252
Pd_3Co-decorated nitrogen/boron-doped graphene	30	298	4.6	253
Phosphorous doped graphene	100	—	2.4	251
Li-decorated holey graphyne	—	—	12.8 (simulation result)	254
Lithium decorated ψ-graphene	—	—	15.15 (simulation result)	255
Ti doped ψ-graphene	—	—	13.14 (simulation result)	256
Zr decorated ψ-graphene	—	—	11.3 (simulation result)	257
Zr-decorated γ-graphyne monolayer	—	—	7.95 (simulation result)	258
Nitrogenated holey graphene (C_2N) with titanium clusters	—	—	6.8	259
3D-graphene	1	77	1.4	260
Transition metal-decorated boron doped twin-graphene	1	77	4.95	261
Lithium doped fullerene pillared graphene nanocomposites (Li-FPGNs)	—	—	9.1	262
Ni/Pd co-modified graphene	4	298	2.65	263
Gold decorated graphene nanosheet	—	—	4.65	264
Diatom frustule-graphene	20	298	4.83	265
Fe–Ti decorated defective graphene	—	—	5.1	266
Ca on graphene	—	—	5–6	
$Mg_{2.3}Y_{0.1}Ni$ alloy with graphene	—	—	3.25	267

g^{-1}), porous structure, and high chemical and thermal stabilities.[243] Pristine graphenes generally have low hydrogen storage capacities while functionalizing graphene nanosheets drastically improve their performance.[244,245] The functionalization includes doping with hetero atoms such as boron (B) and nitrogen (N), decorating with metal atoms, and defect engineering in the nanosheets (Table 2). Moreover, the graphene nanosheets allow surface curvature tuning, which would help develop a reversible hydrogen storage system with enhanced kinetics.[60]

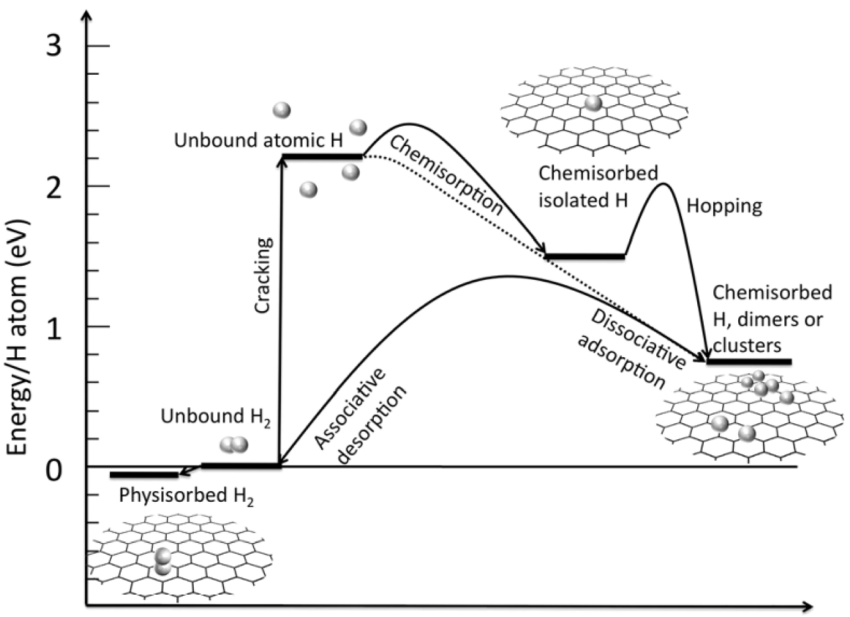

Fig. 13 Energy level diagram of hydrogen adsorption–desorption on the graphene monolayer.[60] Adapted with permission from RSC.

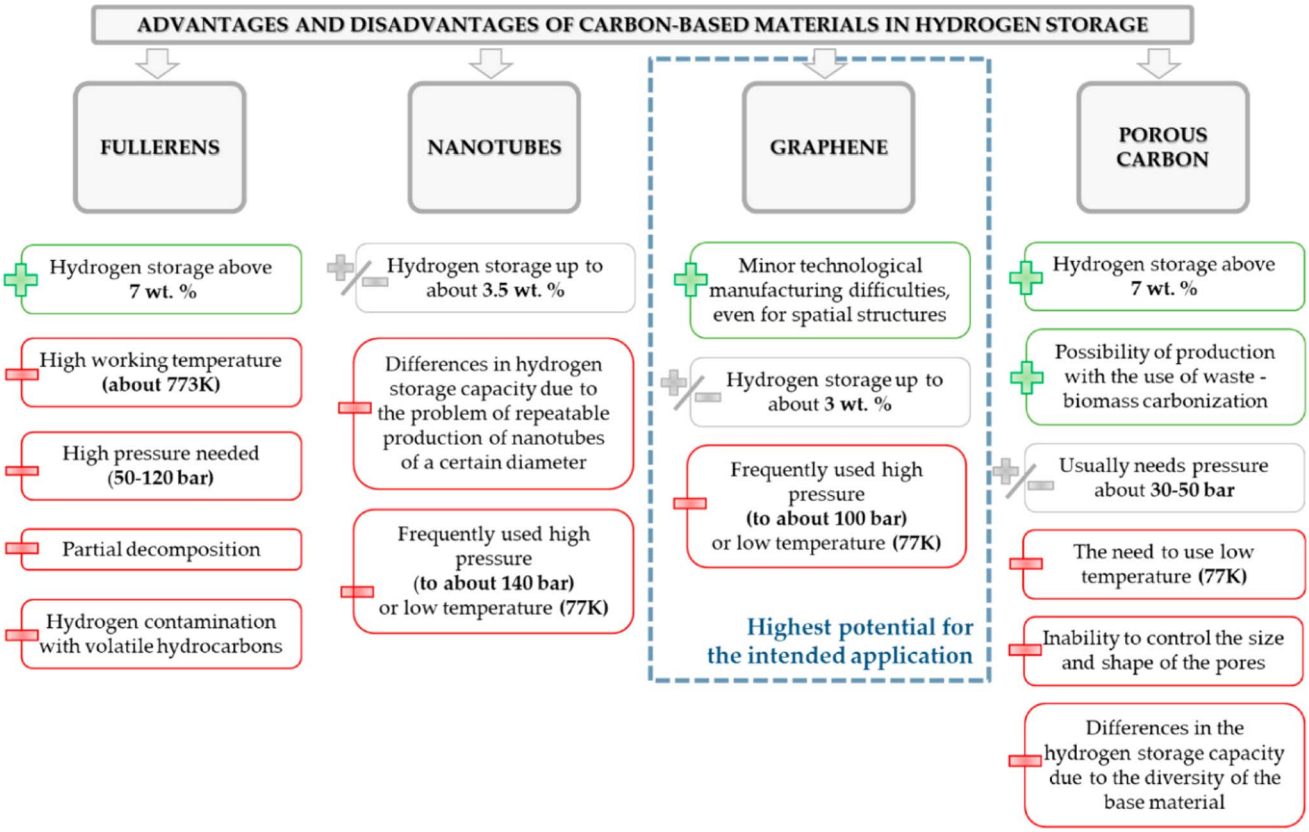

Fig. 14 Summary of solid-state hydrogen storage using different carbon-based materials.[244] Adapted with permission from MDPI.

The adsorption of hydrogen molecules onto graphene sheets can occur either by physisorption (van der Waals interactions) or by chemisorption (chemical bonds with carbon atoms). The theoretical energy requirement for the physisorption of hydrogen molecules (H_2) on single-layer graphenes was evaluated to be in the range of 0.01–0.06 eV (Fig. 13). Even though the energy requirement for hydrogen adsorption onto the graphene sheet is quite low, it still requires low temperatures and high

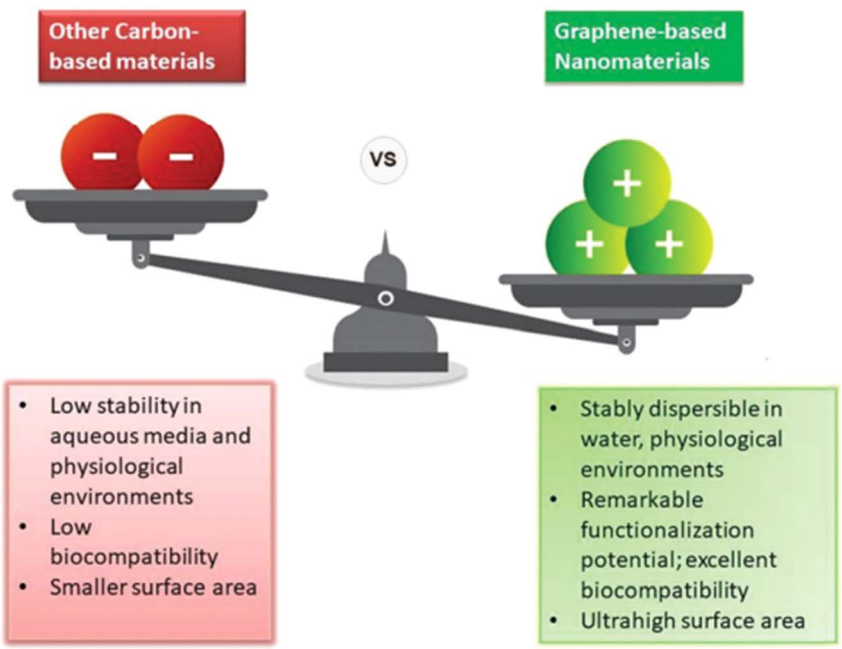

Fig. 15 Advantages of the graphene nanomaterial over other carbon-based nanomaterials. Adapted with permission from RSC.[268]

pressures to achieve reasonable hydrogen storage capacities. Chemisorption requires the dissociation of hydrogen molecules, and consequently, the energy requirement is much higher (1.5 eV) (Fig. 13) than that of physisorption. Hydrogen storage capacities of various graphene-based 2D nanomaterials are summarized in Table 2.

A significant progress has been made in the field of hydrogen storage using graphene-based 2D materials. Among various graphene-based 2D nanomaterials, alkali, alkaline earth, and transition metal nanoparticle-decorated graphene doped with hetero atoms are found to be potential candidates for this purpose. In addition, the functionalized graphene nanosheets are distinctly advantageous than other carbon allotropes such as fullerene, nanotubes, and porous carbons, as shown in Fig. 14. Nevertheless, the adsorption and desorption properties of hydrogen molecules in 2D nanomaterials are still unclear. Therefore, hydrogen storage at ambient temperatures and pressures using functionalized graphene nanosheets even remains a challenge.

5. Summary and outlook

As society's energy needs increase, lithium batteries for energy storage require efficient electrode materials to store energy and the ability to be charged more quickly. Moreover, hydrogen, with the current rate of industrialization leading to greenhouse gas (GHG) emissions, is considered a potential energy carrier that can replace fossil fuels. However, the materials for hydrogen production and storage show challenges of inefficiency and cost-effectiveness. The development of 2D materials may offer a solution to these issues. Graphene is a two-dimensional substance that exhibits remarkable mechanical strength, exceptional conductivity, superb flexibility, high surface area and excellent chemical stability. With these properties, graphenes are desirable for energy storage, hydrogen production and electronic applications (Fig. 15). The synergistic effect of graphenes with 2D composite materials is appropriate for fabricating electrodes of lithium batteries because of their high interlayer adsorption energy and a large specific surface area. As graphenes and 2D composite materials have special features, they can be employed to create stable SEI layers, serve as anode hosts, alter the separator interface (LSB), and change the electrolyte (manage the polysulfides). Additionally, graphenes can enhance the electrical conductivity of two-dimensional materials and lessen volume fluctuations. Apart from this, in terms of H_2 production, GO-based photocatalytic nanocomposites show efficient and economic H_2 generation based on the improved surface area, efficient migration of charges, separation of charges, and provision of active sites. Moreover, in the case of PEC H_2 generation, graphenes show high electric conductivity for efficient charge carrier movement.

Data availability

The data that support the findings of this study are available from the corresponding author.

Conflicts of interest

The manuscript was written with contributions from all authors. All authors have approved the final version of the manuscript.

References

1 Z. Hu, Q. Liu, S.-L. Chou and S.-X. Dou, Two-Dimensional Material-Based Heterostructures for Rechargeable Batteries, *Cell Rep. Phys. Sci.*, 2021, **2**(1), 100286.
2 J. Wang and W. Azam, Natural Resource Scarcity, Fossil Fuel Energy Consumption, and Total Greenhouse Gas Emissions in Top Emitting Countries, *Geosci. Front.*, 2024, **15**(2), 101757.
3 I. H. Shah, M. A. Manzoor, W. Jinhui, X. Li, M. K. Hameed, A. Rehaman, P. Li, Y. Zhang, Q. Niu and L. Chang, Comprehensive Review: Effects of Climate Change and Greenhouse Gases Emission Relevance to Environmental Stress on Horticultural Crops and Management, *J. Environ. Manage.*, 2024, **351**, 119978.
4 M. Shaterabadi, S. Sadeghi and M. A. Jirdehi The Role of Green Hydrogen in Achieving Low and Net-Zero Carbon Emissions: Climate Change and Global Warmin, in *Green Hydrogen in Power Systems*, Springer, 2024, pp. 141–153.
5 R. Lv, C. Luo, B. Liu, K. Hu, K. Wang, L. Zheng, Y. Guo, J. Du, L. Li and F. Wu, Unveiling Confinement Engineering for Achieving High-Performance Rechargeable Batteries, *Adv. Mater.*, 2024, 2400508.
6 S. Wang, L. Wang, S. David, T. Liu, C. Zhan and K. Amine, Correlating Concerted Cations with Oxygen Redox in Rechargeable Batteries, *Chem. Soc. Rev.*, 2024, **53**, 3561–3578.
7 Y.-J. Lei, L. Zhao, W.-H. Lai, Z. Huang, B. Sun, P. Jaumaux, K. Sun, Y.-X. Wang and G. Wang, Electrochemical Coupling in Subnanometer Pores/Channels for Rechargeable Batteries, *Chem. Soc. Rev.*, 2024, **53**, 3829–3895.
8 A. Risco-Bravo, C. Varela, J. Bartels and E. Zondervan, From Green Hydrogen to Electricity: A Review on Recent Advances, Challenges, and Opportunities on Power-to-Hydrogen-to-Power Systems, *Renewable Sustainable Energy Rev.*, 2024, **189**, 113930.
9 F. Frieden and J. Leker, Future Costs of Hydrogen: A Quantitative Review, *Sustainable Energy Fuels*, 2024, **8**, 1806–1822.
10 L. Ge, B. Zhang, W. Huang, Y. Li, L. Hou, J. Xiao, Z. Mao and X. Li, A Review of Hydrogen Generation, Storage, and Applications in Power System, *J. Energy Storage*, 2024, **75**, 109307.
11 B. S. Zainal, P. J. Ker, H. Mohamed, H. C. Ong, I. Fattah, S. A. Rahman, L. D. Nghiem and T. I. Mahlia, Recent Advancement and Assessment of Green Hydrogen Production Technologies, *Renewable Sustainable Energy Rev.*, 2024, **189**, 113941.
12 L. Ruihan, H. Feng, X. Ting, L. Yongzhi, Z. Xin and Z. Jiaqi, Progress in the Application of First Principles to Hydrogen

Storage Materials, *Int. J. Hydrogen Energy*, 2024, **56**, 1079–1091.
13 M. Kurucan, M. Özbaltan, Z. Yetgin and A. Alkaya, Applications of Artificial Neural Network Based Battery Management Systems: A Literature Review, *Renewable Sustainable Energy Rev.*, 2024, **192**, 114262.
14 A. G. Olabi, Q. Abbas, P. A. Shinde and M. A. Abdelkareem, Rechargeable Batteries: Technological Advancement, Challenges, Current and Emerging Applications, *Energy*, 2023, **266**, 126408.
15 F. Mohammadi and M. Saif, A Comprehensive Overview of Electric Vehicle Batteries Market, *e-Prime-Advances in Electrical Engineering, Electronics and Energy*, 2023, **3**, 100127.
16 J. Xu, X. Cai, S. Cai, Y. Shao, C. Hu, S. Lu and S. Ding, High-energy Lithium-ion Batteries: Recent Progress and a Promising Future in Applications, *Energy Environ. Mater.*, 2023, **6**(5), e12450.
17 F. N. U. Khan, M. G. Rasul, A. Sayem and N. K. Mandal, Design and Optimization of Lithium-Ion Battery as an Efficient Energy Storage Device for Electric Vehicles: A Comprehensive Review, *J. Energy Storage*, 2023, **71**, 108033.
18 M. Patel, K. Mishra, R. Banerjee, J. Chaudhari, D. Kanchan and D. Kumar, Fundamentals, Recent Developments and Prospects of Lithium and Non-Lithium Electrochemical Rechargeable Battery Systems, *J. Energy Chem.*, 2023, **81**, 221–259.
19 T. Khan, A. K. Garg, A. Gupta, A. Madan and P. Jain, Comprehensive Review on Latest Advances on Rechargeable Batteries, *J. Energy Storage*, 2023, **57**, 106204.
20 S. Nyamathulla and C. Dhanamjayulu, A Review of Battery Energy Storage Systems and Advanced Battery Management System for Different Applications: Challenges and Recommendations, *J. Energy Storage*, 2024, **86**, 111179.
21 P. Zhang, Social Issues Caused by Lithium-Ion Batteries, *Highl. Sci. Eng. Technol.*, 2024, **83**, 133–138.
22 J. Ke, Y. Zhang, Z. Wen, S. Huang, M. Ye, Y. Tang, X. Liu and C. C. Li, Designing Strategies of Advanced Electrode Materials for High-Rate Rechargeable Batteries, *J. Mater. Chem. A*, 2023, **11**(9), 4428–4457.
23 G. Wang, G. Wang, L. Fei, L. Zhao and H. Zhang, Structural Engineering of Anode Materials for Low-Temperature Lithium-Ion Batteries: Mechanisms, Strategies, and Prospects, *Nano-Micro Lett.*, 2024, **16**(1), 150.
24 Z. Wang, H. Jiang, Y. Zhang, Y. An, C. Wei, L. Tan, S. Xiong, Y. Qian and J. Feng, Application of 2D MXene in Organic Electrode Materials for Rechargeable Batteries: Recent Progress and Perspectives, *Adv. Funct. Mater.*, 2023, **33**(12), 2210184.
25 J. E. G. Baquero and D. B. Monsalve, From Fossil Fuel Energy to Hydrogen Energy: Transformation of Fossil Fuel Energy Economies into Hydrogen Economies through Social Entrepreneurship, *Int. J. Hydrogen Energy*, 2024, **54**, 574–585.
26 T. T. Le, P. Sharma, B. J. Bora, V. D. Tran, T. H. Truong, H. C. Le and P. Q. P. Nguyen, Fueling the Future: A Comprehensive Review of Hydrogen Energy Systems and Their Challenges, *Int. J. Hydrogen Energy*, 2023, **54**, 791–816.
27 Q. Hassan, S. Algburi, A. Z. Sameen, H. M. Salman and M. Jaszczur, Green Hydrogen: A Pathway to a Sustainable Energy Future, *Int. J. Hydrogen Energy*, 2024, **50**, 310–333.
28 M. S. Ali, M. S. Hossain Khan, R. A. Tuhin, M. A. Kabir, A. K. Azad and O. Farrok, Chapter 9 – Hydrogen Energy Storage and Transportation Challenges: A Review of Recent Advances, in *Hydrogen Energy Conversion and Management*, ed. Khan, M. M. K., Azad, A. K. and Oo, A. M. T., Elsevier, 2024, pp. 255–287, DOI: **10.1016/B978-0-443-15329-7.00001-6**.
29 F. Alasali, M. I. Abuashour, W. Hammad, D. Almomani, A. M. Obeidat and W. Holderbaum, A Review of Hydrogen Production and Storage Materials for Efficient Integrated Hydrogen Energy Systems, *Energy Sci. Eng.*, 2024, **12**, 1934–1968.
30 R. Sharma, M. Almáši, S. P. Nehra, V. S. Rao, P. Panchal, D. R. Paul, I. P. Jain and A. Sharma, Photocatalytic Hydrogen Production Using Graphitic Carbon Nitride (GCN): A Precise Review, *Renewable Sustainable Energy Rev.*, 2022, **168**, 112776.
31 L. Zhang, C. Jia, F. Bai, W. Wang, S. An, K. Zhao, Z. Li, J. Li and H. Sun, A Comprehensive Review of the Promising Clean Energy Carrier: Hydrogen Production, Transportation, Storage, and Utilization (HPTSU) Technologies, *Fuel*, 2024, **355**, 129455.
32 R. Singh, A. Altaee and S. Gautam, Nanomaterials in the Advancement of Hydrogen Energy Storage, *Heliyon*, 2020, **6**(7), 04487.
33 F. Xu, J. Ren, J. Ma, Y. Wang, K. Zhang, Z. Cao, Q. Sun, S. Wu, G. Li and S. Bai, A Review of Hydrogen Production Kinetics from the Hydrolysis of NaBH4 Solution Catalyzed by Co-Based Catalysts, *Int. J. Hydrogen Energy*, 2023, **50**, 827–844.
34 N. S. C. Mazlan, M. F. A. A. H. Yap, M. Ismail, M. S. Yahya, N. A. Ali, N. Sazelee and Y. B. Seok, Reinforce the Dehydrogenation Process of LiAlH4 by Accumulating Porous Activated Carbon, *Int. J. Hydrogen Energy*, 2023, **48**(43), 16381–16391.
35 N. Klopčič, I. Grimmer, F. Winkler, M. Sartory and A. Trattner, A Review on Metal Hydride Materials for Hydrogen Storage, *J. Energy Storage*, 2023, **72**, 108456.
36 Ç. Yamçıçıer and C. Kürkçü, Investigation of Structural, Electronic, Elastic, Vibrational, Thermodynamic, and Optical Properties of Mg2NiH4 and Mg2RuH4 Compounds Used in Hydrogen Storage, *J. Energy Storage*, 2024, **84**, 110883.
37 S. Wang, Z. Zhang, Y. Tan, K. Liang and S. Zhang, Review on the Characteristics of Existing Hydrogen Energy Storage Technologies, *Energy Sources, Part A*, 2023, **45**(1), 985–1006.
38 A. Salehabadi, J. Zanganeh and B. Moghtaderi, Mixed Metal Oxides in Catalytic Ammonia Cracking Process for Green Hydrogen Production: A Review, *Int. J. Hydrogen Energy*, 2024, **63**, 828–843.
39 A. Yuvaraj, A. Jayarama, D. Sharma, S. S. Nagarkar, S. P. Duttagupta and R. Pinto, Role of Metal-Organic

Framework in Hydrogen Gas Storage: A Critical Review, *Int. J. Hydrogen Energy*, 2024, **59**, 1434–1458.
40 T. He and Y. Zhao, Covalent Organic Frameworks for Energy Conversion in Photocatalysis, *Angew. Chem., Int. Ed.*, 2023, **62**(34), e202303086.
41 M. Rafique, S. Hajra, M. Irshad, M. Usman, M. Imran, M. A. Assiri and W. M. Ashraf, Hydrogen Production Using TiO2-Based Photocatalysts: A Comprehensive Review, *ACS Omega*, 2023, **8**(29), 25640–25648, DOI: 10.1021/acsomega.3c00963.
42 T. Van Nguyen, M. Tekalgne, T. P. Nguyen, Q. Van Le, S. H. Ahn and S. Y. Kim, Electrocatalysts Based on MoS2 and WS2 for Hydrogen Evolution Reaction: An Overview, *Battery Energy*, 2023, **2**(3), 20220057.
43 Z. Ashfaq, T. Iqbal, H. Ali, S. M. Eldin, F. Al-Harbi, M. Arshad and A. M. Galal, Review of Different CdS/TiO2 and WO3/g-C3N4 Composite Based Photocatalyst for Hydrogen Production, *Arab. J. Chem.*, 2023, 105024.
44 S. K. Nadikatla, V. B. Chintada, T. R. Gurugubelli and R. Koutavarapu, Review of Recent Developments in the Fabrication of ZnO/CdS Heterostructure Photocatalysts for Degradation of Organic Pollutants and Hydrogen Production, *Molecules*, 2023, **28**(11), 4277.
45 M. Damizia, P. J. Lloreda-Jurado, P. De Filippis, B. De Caprariis, E. Chicardi and R. Sepulveda, Green Hydrogen Production Using Doped Fe2O3 Foams, *Int. J. Hydrogen Energy*, 2024, **51**, 834–845.
46 S. Lotfi, M. E. Ouardi, H. A. Ahsaine and A. Assani, Recent Progress on the Synthesis, Morphology and Photocatalytic Dye Degradation of BiVO4 Photocatalysts: A Review, *Catal. Rev.*, 2024, **66**(1), 214–258.
47 D. K. Becerra-Paniagua, S. Torres-Arellano, C. Martinez-Alonso, E. Luévano-Hipólito and P. Sebastian, Facile and Green Synthesis of Cu/Cu2O Composite for Photocatalytic H2 Generation, *Mater. Sci. Semicond. Process.*, 2023, **162**, 107485.
48 C. Prasad, N. Madkhali, J. S. Won, J. E. Lee, S. Sangaraju and H. Y. Choi, CdS Based Heterojunction for Water Splitting: A Review, *Mater. Sci. Eng. B*, 2023, **292**, 116413.
49 L. Clarizia, M. N. Nadagouda and D. D. Dionysiou, Recent Advances and Challenges of Photoelectrochemical Cells for Hydrogen Production, *Curr. Opin. Green Sustainable Chem.*, 2023, **41**, 100825.
50 N. Zhao and J. Wang, Solar Full Spectrum Management in Low and Medium Temperature Light-Driven Chemical Hydrogen Synthesis-A Review, *Renewable Sustainable Energy Rev.*, 2024, **196**, 114368.
51 Z. Chen, Y. Li, L. Wang, Y. Wang, J. Chai, J. Du, Q. Li, Y. Rui, L. Jiang and B. Tang, A Comprehensive Review of Various Carbonaceous Materials for Anode in Lithium-Ion Batteries, *Dalton Trans.*, 2024, **51**, 4900–4921.
52 T.-W. Chen, S.-M. Chen, G. Anushya, R. Kannan, P. Veerakumar, A. G. Al-Sehemi, V. Mariyappan, S. Alargarsamy, M. M. Alam and T. C. Mahesh, Electrochemical Energy Storage Applications of Functionalized Carbon-Based Nanomaterials: An Overview, *Int. J. Electrochem. Sci.*, 2024, 100548.
53 Y. Wang, Z. Zhang, F. Yuan and B. Wang, Design and Modification of Carbon-Based Materials for High Energy Density Non-Aqueous Aluminum Ion Batteries: A Review, *J. Power Sources*, 2024, **597**, 234110.
54 J.-M. Cao, I. V. Zatovsky, Z.-Y. Gu, J.-L. Yang, X.-X. Zhao, J.-Z. Guo, H. Xu and X.-L. Wu, Two-Dimensional MXene with Multidimensional Carbonaceous Matrix: A Platform for General-Purpose Functional Materials, *Prog. Mater. Sci.*, 2023, **135**, 101105, DOI: 10.1016/j.pmatsci.2023.101105.
55 F. Tao, D. Xie, W.-Y. Diao, C. Liu, H.-Z. Sun, W.-L. Li, J.-P. Zhang and X.-L. Wu, Highly Lithiophilic Ti3C2Tx-Mxene Anchored on a Flexible Carbon Foam Scaffolds as the Basis for a Dendrite-Free Lithium Metal Anode, *N. Carbon Mater.*, 2023, **38**(4), 765–773, DOI: 10.1016/S1872-5805(23)60739-5.
56 M. Aizudin, W. Fu, R. P. Pottammel, Z. Dai, H. Wang, X. Rui, J. Zhu, C. C. Li, X.-L. Wu and E. H. Ang, Recent Advancements of Graphene-Based Materials for Zinc-Based Batteries: Beyond Lithium-Ion Batteries, *Small*, 2024, **20**(2), 2305217, DOI: 10.1002/smll.202305217.
57 H. Liu, X. Liu, W. Li, X. Guo, Y. Wang, G. Wang and D. Zhao, Porous Carbon Composites for Next Generation Rechargeable Lithium Batteries, *Adv. Energy Mater.*, 2017, **7**(24), 1700283, DOI: 10.1002/aenm.201700283.
58 W. Yuan, Y. Zhang, L. Cheng, H. Wu, L. Zheng and D. Zhao, The Applications of Carbon Nanotubes and Graphene in Advanced Rechargeable Lithium Batteries, *J. Mater. Chem. A*, 2016, **4**(23), 8932–8951, DOI: 10.1039/C6TA01546H.
59 Q. Xiang and J. Yu, Graphene-Based Photocatalysts for Hydrogen Generation, *J. Phys. Chem. Lett.*, 2013, **4**(5), 753–759.
60 V. Tozzini and V. Pellegrini, Prospects for Hydrogen Storage in Graphene, *Phys. Chem. Chem. Phys.*, 2013, **15**(1), 80–89, DOI: 10.1039/C2CP42538F.
61 B. M. Khan, W. C. Oh, P. Nuengmatch and K. Ullah, Role of Graphene-Based Nanocomposites as Anode Material for Lithium-Ion Batteries, *Mater. Sci. Eng. B*, 2023, **287**, 116141.
62 X. Wang, J. Wang, Z. Chen, K. Yang, Z. Zhang, Z. Shi, T. Mei, J. Qian, J. Li and X. Wang, Yolk-Double Shell Fe3O4@ C@ C Composite as High-Performance Anode Materials for Lithium-Ion Batteries, *J. Alloys Compd.*, 2020, **822**, 153656.
63 D. Deng, Li-ion Batteries: Basics, Progress, and Challenges, *Energy Sci. Eng.*, 2015, **3**(5), 385–418.
64 F. Bonaccorso, L. Colombo, G. Yu, M. Stoller, V. Tozzini, A. C. Ferrari, R. S. Ruoff and V. Pellegrini, Graphene, Related Two-Dimensional Crystals, and Hybrid Systems for Energy Conversion and Storage, *Science*, 2015, **347**(6217), 1246501.
65 E. Morales-Narváez, L. F. Sgobbi, S. A. S. Machado and A. Merkoçi, Graphene-Encapsulated Materials: Synthesis, Applications and Trends, *Prog. Mater. Sci.*, 2017, **86**, 1–24.
66 L. Zhang, X. Qin, S. Zhao, A. Wang, J. Luo, Z. L. Wang, F. Kang, Z. Lin and B. Li, Advanced Matrixes for Binder-free Nanostructured Electrodes in Lithium-ion Batteries, *Adv. Mater.*, 2020, **32**(24), 1908445.

67 M. S. Al Ja'farawy, D. N. Hikmah, U. Riyadi, A. Purwanto and H. Widiyandari, A Review: The Development of SiO 2/C Anode Materials for Lithium-Ion Batteries, *J. Electron. Mater.*, 2021, 1–21.
68 X. Li, X. Sun, X. Hu, F. Fan, S. Cai, C. Zheng and G. D. Stucky, Review on Comprehending and Enhancing the Initial Coulombic Efficiency of Anode Materials in Lithium-Ion/Sodium-Ion Batteries, *Nano Energy*, 2020, **77**, 105143.
69 H. Lin, N. Lou, D. Yang, R. Jin and Y. Huang, Janus MoSSe/Graphene Heterostructures: Potential Anodes for Lithium-Ion Batteries, *J. Alloys Compd.*, 2021, **854**, 157215.
70 S. Dhar, T. Dash, B. Palei, T. Rout, S. Biswal, A. Mitra and A. Sahu, Silicon-Graphene Composite Synthesis: Microstructural, Spectroscopic and Electrical Conductivity Characterizations, *Mater. Today: Proc.*, 2020, **33**, 5136–5142.
71 X. Zhao, E. Jiaqiang, G. Wu, Y. Deng, D. Han, B. Zhang and Z. Zhang, A Review of Studies Using Graphenes in Energy Conversion, Energy Storage and Heat Transfer Development, *Energy Convers. Manage.*, 2019, **184**, 581–599.
72 K. Wu, H. Yang, L. Jia, Y. Pan, Y. Hao, K. Zhang, K. Du and G. Hu, Smart Construction of 3D N-Doped Graphene Honeycombs with (NH 4) 2 SO 4 as a Multifunctional Template for Li-Ion Battery Anode:"A Choice That Serves Three Purposes.", *Green Chem.*, 2019, **21**(6), 1472–1483.
73 Z.-S. Wu, G. Zhou, L.-C. Yin, W. Ren, F. Li and H.-M. Cheng, Graphene/Metal Oxide Composite Electrode Materials for Energy Storage, *Nano Energy*, 2012, **1**(1), 107–131.
74 N. Li, Z. Chen, W. Ren, F. Li and H.-M. Cheng, Flexible Graphene-Based Lithium Ion Batteries with Ultrafast Charge and Discharge Rates, *Proc. Natl. Acad. Sci. U. S. A.*, 2012, **109**(43), 17360–17365.
75 J. Shao, J. Feng, H. Zhou and A. Yuan, Graphene Aerogel Encapsulated Fe-Co Oxide Nanocubes Derived from Prussian Blue Analogue as Integrated Anode with Enhanced Li-Ion Storage Properties, *Appl. Surf. Sci.*, 2019, **471**, 745–752.
76 N. Antonatos, H. Ghodrati and Z. Sofer, Elements beyond Graphene: Current State and Perspectives of Elemental Monolayer Deposition by Bottom-up Approach, *Appl. Mater. Today*, 2020, **18**, 100502.
77 R. Mo, X. Tan, F. Li, R. Tao, J. Xu, D. Kong, Z. Wang, B. Xu, X. Wang and C. Wang, Tin-Graphene Tubes as Anodes for Lithium-Ion Batteries with High Volumetric and Gravimetric Energy Densities, *Nat. Commun.*, 2020, **11**(1), 1374.
78 K. Ullah, L. Zhu, Z.-D. Meng, S. Ye, S. Sarkar and W.-C. Oh, Synthesis and Characterization of Novel PtSe 2/Graphene Nanocomposites and Its Visible Light Driven Catalytic Properties, *J. Mater. Sci.*, 2014, **49**, 4139–4147.
79 S. Z. Hussain, M. Ihrar, S. B. Hussain, W. C. Oh and K. Ullah, A Review on Graphene Based Transition Metal Oxide Composites and Its Application towards Supercapacitor Electrodes, *SN Appl. Sci.*, 2020, **2**, 1–23.
80 X. Yu, J. Tang, K. Terabe, T. Sasaki, R. Gao, Y. Ito, K. Nakura, K. Asano and M. Suzuki, Fabrication of Graphene/MoS2 Alternately Stacked Structure for Enhanced Lithium Storage, *Mater. Chem. Phys.*, 2020, **239**, 121987.
81 Z.-S. Wu, W. Ren, L. Xu, F. Li and H.-M. Cheng, Doped Graphene Sheets as Anode Materials with Superhigh Rate and Large Capacity for Lithium Ion Batteries, *ACS Nano*, 2011, **5**(7), 5463–5471.
82 M. Mazar Atabaki and R. Kovacevic, Graphene Composites as Anode Materials in Lithium-Ion Batteries, *Electron. Mater. Lett.*, 2013, **9**, 133–153.
83 Y. Gong, S. Yang, Z. Liu, L. Ma, R. Vajtai and P. M. Ajayan, Graphene-network-backboned Architectures for High-performance Lithium Storage, *Adv. Mater.*, 2013, **25**(29), 3979–3984.
84 N. Chodankar, A. Nanjundan, D. Losic, D. Dubal and J.-B. Baek, Graphene and Molybdenum Disulphide Hybrids for Energy Applications: An Update, *Mater. Today Adv.*, 2020, **6**, 100053.
85 J. Xiao, D. Mei, X. Li, W. Xu, D. Wang, G. L. Graff, W. D. Bennett, Z. Nie, L. V. Saraf and I. A. Aksay, Hierarchically Porous Graphene as a Lithium–Air Battery Electrode, *Nano Lett.*, 2011, **11**(11), 5071–5078.
86 Y. Fang, Y. Lv, R. Che, H. Wu, X. Zhang, D. Gu, G. Zheng and D. Zhao, Two-Dimensional Mesoporous Carbon Nanosheets and Their Derived Graphene Nanosheets: Synthesis and Efficient Lithium Ion Storage, *J. Am. Chem. Soc.*, 2013, **135**(4), 1524–1530, DOI: **10.1021/ja310849c**.
87 X. Zhu, J. Ye, Y. Lu and X. Jia, 3D Graphene Nanostructure Composed of Porous Carbon Sheets and Interconnected Nanocages for High-Performance Lithium-Ion Battery Anodes and Lithium–Sulfur Batteries, *ACS Sustain. Chem. Eng.*, 2019, **7**(13), 11241–11249.
88 P.-M. Ting, J.-Y. Huang, R. Murugananthan and W.-R. Liu, Nitrogen-Doping Effects on Few-Layer Graphene as an Anode Material for Lithium-Ion Batteries, *Mater. Today Commun.*, 2022, **31**, 103498, DOI: **10.1016/j.mtcomm.2022.103498**.
89 Y. S. Yun, V.-D. Le, H. Kim, S.-J. Chang, S. J. Baek, S. Park, B. H. Kim, Y.-H. Kim, K. Kang and H.-J. Jin, Effects of Sulfur Doping on Graphene-Based Nanosheets for Use as Anode Materials in Lithium-Ion Batteries, *J. Power Sources*, 2014, **262**, 79–85.
90 D. Cai, C. Wang, C. Shi and N. Tan, Facile Synthesis of N and S Co-Doped Graphene Sheets as Anode Materials for High-Performance Lithium-Ion Batteries, *J. Alloys Compd.*, 2018, **731**, 235–242, DOI: **10.1016/j.jallcom.2017.10.043**.
91 C. Zhang, N. Mahmood, H. Yin, F. Liu and Y. Hou, Synthesis of Phosphorus-doped Graphene and Its Multifunctional Applications for Oxygen Reduction Reaction and Lithium Ion Batteries, *Adv. Mater.*, 2013, **25**(35), 4932–4937.
92 R. Bhushan, P. Kumar and A. K. Thakur, Catalyst-Free Solvothermal Synthesis of Ultrapure Elemental N- and B-Doped Graphene for Energy Storage Application, *Solid State Ionics*, 2020, **353**, 115371, DOI: **10.1016/j.ssi.2020.115371**.
93 X. Lang, X. Wang, Y. Liu, K. Cai, L. Li and Q. Zhang, Cobalt-based Metal Organic Framework (Co-MOFs)/

Graphene Oxide Composites as High-performance Anode Active Materials for Lithium-ion Batteries, *Int. J. Energy Res.*, 2021, **45**(3), 4811–4820.

94 C. Liu, Y. Bai, Y. Zhao, H. Yao and H. Pang, MoS2/Graphene Composites: Fabrication and Electrochemical Energy Storage, *Energy Storage Mater.*, 2020, **33**, 470–502.

95 S. Wang, Y. Shi, C. Fan, J. Liu, Y. Li, X.-L. Wu, H. Xie, J. Zhang and H. Sun, Layered G-C3N4@ Reduced Graphene Oxide Composites as Anodes with Improved Rate Performance for Lithium-Ion Batteries, *ACS Appl. Mater. Interfaces*, 2018, **10**(36), 30330–30336.

96 D. Adekoya, S. Zhang and M. Hankel, 1D/2D C3N4/Graphene Composite as a Preferred Anode Material for Lithium Ion Batteries: Importance of Heterostructure Design via DFT Computation, *ACS Appl. Mater. Interfaces*, 2020, **12**(23), 25875–25883.

97 J. R. Rodriguez, P. J. Kim, K. Kim, Z. Qi, H. Wang and V. G. Pol, Engineered Heat Dissipation and Current Distribution Boron Nitride-Graphene Layer Coated on Polypropylene Separator for High Performance Lithium Metal Battery, *J. Colloid Interface Sci.*, 2021, **583**, 362–370, DOI: **10.1016/j.jcis.2020.09.009**.

98 S. F. Zhao, G. A. Elbaz, D. K. Bediako, C. Yu, D. K. Efetov, Y. Guo, J. Ravichandran, K.-A. Min, S. Hong and T. Taniguchi, Controlled Electrochemical Intercalation of Graphene/h-BN van Der Waals Heterostructures, *Nano Lett.*, 2018, **18**(1), 460–466.

99 H. Li, R. Y. Tay, S. H. Tsang, W. Liu and E. H. T. Teo, Reduced Graphene Oxide/Boron Nitride Composite Film as a Novel Binder-Free Anode for Lithium Ion Batteries with Enhanced Performances, *Electrochim. Acta*, 2015, **166**, 197–205.

100 J. Hong, A.-R. Jang, W. B. Park, B. Hou, J.-O. Lee, K.-S. Sohn, S. Cha, Y.-W. Lee and J. I. Sohn, Thermodynamically and Physically Stable Dendrite-Free Li Interface with Layered Boron Nitride Separators, *ACS Sustain. Chem. Eng.*, 2021, **9**(11), 4185–4193.

101 D. He, Y. Yang, Z. Liu, J. Shao, J. Wu, S. Wang, L. Shen and N. Bao, Solvothermal-Assisted Assembly of MoS 2 Nanocages on Graphene Sheets to Enhance the Electrochemical Performance of Lithium-Ion Battery, *Nano Res.*, 2020, **13**, 1029–1034.

102 Z. Ma, X. Zhou, W. Deng, D. Lei and Z. Liu, 3D Porous MXene (Ti3C2)/Reduced Graphene Oxide Hybrid Films for Advanced Lithium Storage, *ACS Appl. Mater. Interfaces*, 2018, **10**(4), 3634–3643, DOI: **10.1021/acsami.7b17386**.

103 H. Shi, C. J. Zhang, P. Lu, Y. Dong, P. Wen and Z.-S. Wu, Conducting and Lithiophilic MXene/Graphene Framework for High-Capacity, Dendrite-Free Lithium–Metal Anodes, *ACS Nano*, 2019, **13**(12), 14308–14318, DOI: **10.1021/acsnano.9b07710**.

104 B. Zhang, Z. Ju, Q. Xie, J. Luo, L. Du, C. Zhang and X. Tao, Ti3CNTx MXene/rGO Scaffolds Directing the Formation of a Robust, Layered SEI toward High-Rate and Long-Cycle Lithium Metal Batteries, *Energy Storage Mater.*, 2023, **58**, 322–331, DOI: **10.1016/j.ensm.2023.03.030**.

105 X. Zhou, X. Lan, Z. Jiao, H. Zong, P. Zhang and B. Xu, High-Content 1T Phase MoS2 Nanosheets Coupled on Graphene Oxide for Lithium-Ion Batteries, *J. Alloys Compd.*, 2024, **971**, 172640, DOI: **10.1016/j.jallcom.2023.172640**.

106 Y.-M. Gao, Y. Liu, K.-J. Feng, J.-Q. Ma, Y.-J. Miao, B.-R. Xu, K.-M. Pan, O. Akiyoshi, G.-X. Wang and K.-K. Zhang, Emerging WS2/WSe2@ Graphene Nanocomposites: Synthesis and Electrochemical Energy Storage Applications, *Rare Met.*, 2024, **43**(1), 1–19.

107 Y.-L. Wu, J.-B. Hong, W.-X. Zhong, C.-X. Wang, Z.-F. Li and S. Dmytro, Auxiliary Ball Milling to Prepare WS2/Graphene Nanosheets Composite for Lithium-Ion Battery Anode Materials, *Tungsten*, 2023, 1–10.

108 Y.-T. Du, X. Kan, F. Yang, L.-Y. Gan and U. Schwingenschlögl, MXene/Graphene Heterostructures as High-Performance Electrodes for Li-Ion Batteries, *ACS Appl. Mater. Interfaces*, 2018, **10**(38), 32867–32873.

109 M. S. Mohseni-Salehi, E. Taheri-Nassaj, A. Babaei, A. S. Ghazvini and M. Soleimanzade, V2CTx-carbon Nanotube/Graphene Nanohybrids for Li-Ion Storage Applications, *J. Energy Storage*, 2024, **85**, 111033, DOI: **10.1016/j.est.2024.111033**.

110 J. Aslam and Y. Wang, Metal Oxide Wrapped by Reduced Graphene Oxide Nanocomposites as Anode Materials for Lithium-Ion Batteries, *Nanomaterials*, 2023, **13**(2), 296.

111 K. Ullah, N. Shah, R. Wadood, B. M. Khan and W. C. Oh, Recent Trends in Graphene Based Transition Metal Oxides as Anode Materials for Rechargeable Lithium-Ion Batteries, *NanoTrends*, 2023, **1**, 100004.

112 E. Muchuweni, E. T. Mombeshora, C. M. Muiva and T. S. Sathiaraj, Lithium-Ion Batteries: Recent Progress in Improving the Cycling and Rate Performances of Transition Metal Oxide Anodes by Incorporating Graphene-Based Materials, *J. Energy Storage*, 2023, **73**, 109013, DOI: **10.1016/j.est.2023.109013**.

113 W. Teng, Z. Lu, X. Li, X. wang, J. Liu, J. Dong and D. Nan, High-Performance Flexible SnO2 Anode Boosted by an N-Doped Graphite Coating Layer for Lithium-Ion and Sodium-Ion Batteries, *Electrochem. Commun.*, 2022, **141**, 107345, DOI: **10.1016/j.elecom.2022.107345**.

114 T. Liu, Y. Guo, S. Hou, W. Fu, J. Li, L. Meng, C. Mei and L. Zhao, Constructing Hierarchical ZnO@C Composites Using Discarded Sprite and Fanta Drinks for Enhanced Lithium Storage, *Appl. Surf. Sci.*, 2021, **541**, 148495, DOI: **10.1016/j.apsusc.2020.148495**.

115 S. Zhu, B. Liang, X. Mou, X. Liang, H. Huang, D. Huang, W. Zhou, S. Xu and J. Guo, In-Situ Synthesis of F-Doped FeOOH Nanorods on Graphene as Anode Materials for High Lithium Storage, *J. Alloys Compd.*, 2022, **905**, 164142, DOI: **10.1016/j.jallcom.2022.164142**.

116 X. Lv, Z. Deng, M. Wang and J. Deng, Ti3C2 MXene Derived Carbon-Doped TiO2 Multilayers Anchored with Fe2O3 Nanoparticles as Anode for Enhanced Lithium-Ion Storage, *J. Alloys Compd.*, 2022, **918**, 165697, DOI: **10.1016/j.jallcom.2022.165697**.

117 N. Muhammad, G. Yasin, A. Li, Y. Chen, H. M. Saleem, R. Liu, D. Li, Y. Sun, S. Zheng, X. Chen and H. Song,

Volumetric Buffering of Manganese Dioxide Nanotubes by Employing 'as Is' Graphene Oxide: An Approach towards Stable Metal Oxide Anode Material in Lithium-Ion Batteries, *J. Alloys Compd.*, 2020, **842**, 155803, DOI: 10.1016/j.jallcom.2020.155803.

118 L. Tan, X. Lan, R. Hu, J. Liu, B. Yuan and M. Zhu, Stable Lithium Storage at Subzero Temperatures for High-capacity Co3O4@ Graphene Composite Anodes, *ChemNanoMat*, 2021, **7**(1), 61–70.

119 Y. Huang, Y. Li, R. Huang, J. Ji, J. Yao and S. Xiao, One-Pot Hydrothermal Synthesis of N-rGO Supported Fe2O3 Nanoparticles as a Superior Anode Material for Lithium-Ion Batteries, *Solid State Ionics*, 2021, **368**, 115693, DOI: 10.1016/j.ssi.2021.115693.

120 L. Fan, Y. Zhang, H. Zhou, Z. Guo, Y. Feng and N. Zhang, Kinetically Enhanced Electrochemical Redox Reactions by Chemical Bridging SnO2 and Graphene Sponges toward High-Rate and Long-Cycle Lithium Ion Battery, *J. Mater. Sci. Technol.*, 2021, **88**, 250–257, DOI: 10.1016/j.jmst.2020.11.082.

121 J. Fu, W. Kang, X. Guo, H. Wen, T. Zeng, R. Yuan and C. Zhang, 3D Hierarchically Porous NiO/Graphene Hybrid Paper Anode for Long-Life and High Rate Cycling Flexible Li-Ion Batteries, *J. Energy Chem.*, 2020, **47**, 172–179.

122 P. M. Ette, D. Bosubabu and K. Ramesha, Graphene Anchored Mesoporous MnO2 Nanostructures as Stable and High-Performance Anode Materials for Li-Ion Batteries, *Electrochim. Acta*, 2022, **414**, 140164, DOI: 10.1016/j.electacta.2022.140164.

123 J. Xu, D. Xu, J. Wu, J. Wu, J. Zhou, T. Zhou, X. Wang and J. P. Cheng, Ultra-Small Fe2O3 Nanoparticles Anchored on Ultrasonically Exfoliated Multilayer Graphene for LIB Anode Application, *Ceram. Int.*, 2022, **48**(21), 32524–32531, DOI: 10.1016/j.ceramint.2022.07.198.

124 S. Jiang, M. Mao, M. Pang, H. Yang, R. Wang, N. LI, Q. Pan, M. Pang and J. Zhao, Preparation and Performance of a Graphene-(Ni-NiO)-C Hybrid as the Anode of a Lithium-Ion Battery, *N. Carbon Mater.*, 2023, **38**(2), 356–365, DOI: 10.1016/S1872-5805(22)60647-4.

125 C. Bi, M. Zhao, L. Hou, Z. Chen, X. Zhang, B. Li, H. Yuan and J. Huang, Anode Material Options toward 500 W h Kg− 1 Lithium–Sulfur Batteries, *Adv. Sci.*, 2022, **9**(2), 2103910.

126 Y. Huang, L. Lin, C. Zhang, L. Liu, Y. Li, Z. Qiao, J. Lin, Q. Wei, L. Wang and Q. Xie, Recent Advances and Strategies toward Polysulfides Shuttle Inhibition for High-performance Li–S Batteries, *Adv. Sci.*, 2022, **9**(12), 2106004.

127 D. R. Deng, F. Xue, C.-D. Bai, J. Lei, R. Yuan, M. S. Zheng and Q. F. Dong, Enhanced Adsorptions to Polysulfides on Graphene-Supported BN Nanosheets with Excellent Li–S Battery Performance in a Wide Temperature Range, *ACS Nano*, 2018, **12**(11), 11120–11129, DOI: 10.1021/acsnano.8b05534.

128 B. Yu, Y. Fan, S. Mateti, D. Kim, C. Zhao, S. Lu, X. Liu, Q. Rong, T. Tao and K. K. Tanwar, An Ultra-Long-Life Flexible Lithium–Sulfur Battery with Lithium Cloth Anode and Polysulfone-Functionalized Separator, *ACS Nano*, 2020, **15**(1), 1358–1369.

129 D.-R. Deng, C.-D. Bai, F. Xue, J. Lei, P. Xu, M.-S. Zheng and Q.-F. Dong, Multifunctional Ion-Sieve Constructed by 2D Materials as an Interlayer for Li–S Batteries, *ACS Appl. Mater. Interfaces*, 2019, **11**(12), 11474–11480.

130 J. Zhang, J. Li, W. Wang, X. Zhang, X. Tan, W. Chu and Y. Guo, Microemulsion Assisted Assembly of 3D Porous s/Graphene@ g-C3N4 Hybrid Sponge as Free-standing Cathodes for High Energy Density Li–S Batteries, *Adv. Energy Mater.*, 2018, **8**(14), 1702839.

131 L. Qu, P. Liu, Y. Yi, T. Wang, P. Yang, X. Tian, M. Li, B. Yang and S. Dai, Enhanced Cycling Performance for Lithium–Sulfur Batteries by a Laminated 2D g-C3N4/Graphene Cathode Interlayer, *ChemSusChem*, 2019, **12**(1), 213–223.

132 X. Wu, S. Li, B. Wang, J. Liu and M. Yu, Free-Standing 3D Network-like Cathode Based on Biomass-Derived N-Doped Carbon/Graphene/g-C3N4 Hybrid Ultrathin Sheets as Sulfur Host for High-Rate Li-S Battery, *Renew. Energy*, 2020, **158**, 509–519.

133 J. Nan, X. Guo, J. Xiao, X. Li, W. Chen, W. Wu, H. Liu, Y. Wang, M. Wu and G. Wang, Nanoengineering of 2D MXene-based Materials for Energy Storage Applications, *Small*, 2021, **17**(9), 1902085.

134 M. Shekhirev, C. E. Shuck, A. Sarycheva and Y. Gogotsi, Characterization of MXenes at Every Step, from Their Precursors to Single Flakes and Assembled Films, *Prog. Mater. Sci.*, 2021, **120**, 100757.

135 Q. Zhong, Y. Li and G. Zhang, Two-Dimensional MXene-Based and MXene-Derived Photocatalysts: Recent Developments and Perspectives, *Chem. Eng. J.*, 2021, **409**, 128099.

136 F. Zhang, Y. Zhou, Y. Zhang, D. Li and Z. Huang, Facile Synthesis of Sulfur@ Titanium Carbide MXene as High Performance Cathode for Lithium-Sulfur Batteries, *Nanophotonics*, 2020, **9**(7), 2025–2032.

137 L. Yuanzheng, Y. Zhicheng, M. Lianghao, L. Buyin and L. Shufa, A Freestanding Nitrogen-Doped MXene/Graphene Cathode for High-Performance Li–S Batteries, *Nanoscale Adv.*, 2022, **4**(9), 2189–2195.

138 S. Nam, J. Kim, V. H. Nguyen, M. Mahato, S. Oh, P. Thangasamy, C. W. Ahn and I. Oh, Collectively Exhaustive MXene and Graphene Oxide Multilayer for Suppressing Shuttling Effect in Flexible Lithium Sulfur Battery, *Adv. Mater. Technol.*, 2022, **7**(5), 2101025.

139 J. He, G. Hartmann, M. Lee, G. S. Hwang, Y. Chen and A. Manthiram, Freestanding 1T MoS 2/Graphene Heterostructures as a Highly Efficient Electrocatalyst for Lithium Polysulfides in Li–S Batteries, *Energy Environ. Sci.*, 2019, **12**(1), 344–350.

140 Z. Wei, S. Sarwar, S. Azam, M. R. Ahasan, M. Voyda, X. Zhang and R. Wang, Ultrafast Microwave Synthesis of MoTe2@graphene Composites Accelerating Polysulfide Conversion and Promoting Li2S Nucleation for High-Performance Li-S Batteries, *J. Colloid Interface Sci.*, 2023, **635**, 391–405, DOI: 10.1016/j.jcis.2022.12.111.

141 J. Zhang, G. Xu, Q. Zhang, X. Li, Y. Yang, L. Yang, J. Huang and G. Zhou, Mo-O-C Between MoS2 and Graphene Toward Accelerated Polysulfide Catalytic Conversion for Advanced Lithium-Sulfur Batteries, *Adv. Sci.*, 2022, **9**(22), 2201579.
142 X. Fang and M. Zhang, MoS 2/G Interlayer as a Polysulfide Immobilization Apparatus for High-Performance Lithium–Sulfur Batteries, *Ionics*, 2021, **27**, 3875–3885.
143 Y. Feng, H. Liu, Y. Liu, F. Zhao, J. Li and X. He, Defective TiO2-Graphene Heterostructures Enabling in-Situ Electrocatalyst Evolution for Lithium-Sulfur Batteries, *J. Energy Chem.*, 2021, **62**, 508–515.
144 Z. Xiao, Z. Yang, L. Wang, H. Nie, M. Zhong, Q. Lai, X. Xu, L. Zhang and S. Huang, Lithium-Sulfur Batteries: A Lightweight TiO2/Graphene Interlayer, Applied as a Highly Effective Polysulfide Absorbent for Fast, Long-Life Lithium–Sulfur Batteries (Adv. Mater. 18/2015), *Adv. Mater.*, 2015, **27**(18), 2890.
145 J. Li, Y. Xu, W. Hou and X. Yao, Loading Fe3O4 Nanoparticles on N, S Co-Doped Graphene Suppressing Polysulfides Conversion toward High-Performance Li–S Batteries, *J. Mater. Sci.*, 2023, **58**(10), 4552–4564.
146 P. G. Bruce, S. A. Freunberger, L. J. Hardwick and J.-M. Tarascon, Li–O2 and Li–S Batteries with High Energy Storage, *Nat. Mater.*, 2012, **11**(1), 19–29.
147 D. Geng, N. Ding, T. A. Hor, S. W. Chien, Z. Liu, D. Wuu, X. Sun and Y. Zong, From Lithium-oxygen to Lithium-air Batteries: Challenges and Opportunities, *Adv. Energy Mater.*, 2016, **6**(9), 1502164.
148 A. Ahmadiparidari, R. E. Warburton, L. Majidi, M. Asadi, A. Chamaani, J. R. Jokisaari, S. Rastegar, Z. Hemmat, B. Sayahpour and R. S. Assary, A Long-cycle-life Lithium–CO2 Battery with Carbon Neutrality, *Adv. Mater.*, 2019, **31**(40), 1902518.
149 L. Majidi, P. Yasaei, R. E. Warburton, S. Fuladi, J. Cavin, X. Hu, Z. Hemmat, S. B. Cho, P. Abbasi and M. Vörös, New Class of Electrocatalysts Based on 2D Transition Metal Dichalcogenides in Ionic Liquid, *Adv. Mater.*, 2019, **31**(4), 1804453.
150 M. Carboni, A. G. Marrani, R. Spezia and S. Brutti, Degradation of LiTfO/TEGME and LiTfO/DME Electrolytes in Li-O2 Batteries, *J. Electrochem. Soc.*, 2018, **165**(2), A118.
151 M. D. Bhatt, H. Geaney, M. Nolan and C. O'Dwyer, Key Scientific Challenges in Current Rechargeable Non-Aqueous Li–O 2 Batteries: Experiment and Theory, *Phys. Chem. Chem. Phys.*, 2014, **16**(24), 12093–12130.
152 R. Rojaee and R. Shahbazian-Yassar, Two-Dimensional Materials to Address the Lithium Battery Challenges, *ACS Nano*, 2020, **14**(3), 2628–2658.
153 F. Su, X. Hou, J. Qin and Z. Wu, Recent Advances and Challenges of Two-dimensional Materials for High-energy and High-power Lithium-ion Capacitors, *Batteries Supercaps*, 2020, **3**(1), 10–29.
154 E. Pomerantseva and Y. Gogotsi, Two-Dimensional Heterostructures for Energy Storage, *Nat. Energy*, 2017, **2**(7), 1–6.
155 H. Tian, Z. W. Seh, K. Yan, Z. Fu, P. Tang, Y. Lu, R. Zhang, D. Legut, Y. Cui and Q. Zhang, Theoretical Investigation of 2D Layered Materials as Protective Films for Lithium and Sodium Metal Anodes, *Adv. Energy Mater.*, 2017, **7**(13), 1602528.
156 L. Zhu, F. Scheiba, V. Trouillet, M. Georgian, Q. Fu, A. Sarapulpva, F. Sigel, W. Hua and H. Ehrenberg, MnO2 and Reduced Graphene Oxide as Bifunctional Electrocatalysts for Li–O2 Batteries, *ACS Appl. Energy Mater.*, 2019, **2**(10), 7121–7131, DOI: **10.1021/acsaem.9b01047**.
157 Y. Li, J. Qin, Y. Ding, J. Ma, P. Das, H. Liu, Z.-S. Wu and X. Bao, Two-Dimensional Mn3O4 Nanosheets with Dominant (101) Crystal Planes on Graphene as Efficient Oxygen Catalysts for Ultrahigh Capacity and Long-Life Li–O2 Batteries, *ACS Catal.*, 2022, **12**(20), 12765–12773, DOI: **10.1021/acscatal.2c02544**.
158 W. Zhao, Y. Yang, Q. Deng, Q. Dai, Z. Fang, X. Fu, W. Yan, L. Wu and Y. Zhou, Toward an Understanding of Bimetallic MXene Solid-Solution in Binder-Free Electrocatalyst Cathode for Advanced Li–CO2 Batteries, *Adv. Funct. Mater.*, 2023, **33**(5), 2210037.
159 F. Liu, J. Zhou, Y. Wang, Y. Xiong, F. Hao, Y. Ma, P. Lu, J. Wang, J. Yin and G. Wang, Rational Engineering of 2D Materials as Advanced Catalyst Cathodes for High-Performance Metal–Carbon Dioxide Batteries, *Small Struct.*, 2023, **4**(9), 2300025.
160 W. Yu, L. Liu, Y. Yang, N. Li, Y. Chen, X. Yin, J. Niu, J. Wang and S. N. Ding, O-Diatomic Dopants Activate Catalytic Activity of 3D Self-Standing Graphene Carbon Aerogel for Long-Cycle and High-Efficiency Li-CO2 Batteries, *Chem. Eng. J.*, 2023, **465**, 142787, DOI: **10.1016/j.cej.2023.142787**.
161 Y. Jiao, J. Qin, H. M. K. Sari, D. Li, X. Li and X. Sun, Recent Progress and Prospects of Li-CO2 Batteries: Mechanisms, Catalysts and Electrolytes, *Energy Storage Mater.*, 2021, **34**, 148–170, DOI: **10.1016/j.ensm.2020.09.014**.
162 Z. Zhang, Q. Zhang, Y. Chen, J. Bao, X. Zhou, Z. Xie, J. Wei and Z. Zhou, The First Introduction of Graphene to Rechargeable Li–CO2 Batteries, *Angew. Chem.*, 2015, **127**(22), 6650–6653.
163 B. Wu, S. Wang, J. Lochala, D. Desrochers, B. Liu, W. Zhang, J. Yang and J. Xiao, The Role of the Solid Electrolyte Interphase Layer in Preventing Li Dendrite Growth in Solid-State Batteries, *Energy Environ. Sci.*, 2018, **11**(7), 1803–1810, DOI: **10.1039/C8EE00540K**.
164 W. Liu, Y. Xia, W. Wang, Y. Wang, J. Jin, Y. Chen, E. Paek and D. Mitlin, Pristine or Highly Defective? Understanding the Role of Graphene Structure for Stable Lithium Metal Plating, *Adv. Energy Mater.*, 2019, **9**(3), 1802918, DOI: **10.1002/aenm.201802918**.
165 S. Shi, D. Zhou, Y. Jiang, F. Cheng, J. Sun, Q. Guo, Y. Luo, Y. Chen and W. Liu, Lightweight Zn-Philic 3D-Cu Scaffold for Customizable Zinc Ion Batteries, *Adv. Funct. Mater.*, 2024, **34**(24), 2312664, DOI: **10.1002/adfm.202312664**.
166 H. Xu, Y. He, Z. Zhang, J. Shi, P. Liu, Z. Tian, K. Luo, X. Zhang, S. Liang and Z. Liu, Slurry-like Hybrid Electrolyte with High Lithium-Ion Transference Number for Dendrite-Free Lithium Metal Anode, *J. Energy Chem.*, 2020, **48**, 375–382, DOI: **10.1016/j.jechem.2020.02.009**.

167 M. Li, X. Liu, Q. Li, Z. Jin, W. Wang, A. Wang, Y. Huang and Y. Yang, P4S10 Modified Lithium Anode for Enhanced Performance of Lithium–Sulfur Batteries, *J. Energy Chem.*, 2020, **41**, 27–33, DOI: 10.1016/j.jechem.2019.03.038.

168 Z. Yao, W. Li, T. Chen, X. Xu and Q. Xiao, Recent Progress on Nanomodification Applied in Anodes of Rechargeable Li Metal Batteries, *ACS Appl. Energy Mater.*, 2023, **6**(20), 10518–10541, DOI: 10.1021/acsaem.3c01657.

169 J.-F. Ding, R. Xu, C. Yan, Y. Xiao, L. Xu, H.-J. Peng, H. S. Park, J. Liang and J.-Q. Huang, Review on Nanomaterials for Next-Generation Batteries with Lithium Metal Anodes, *Nano Sel.*, 2020, **1**(1), 94–110, DOI: 10.1002/nano.202000003.

170 P. Jiang, Y. Liao, W. Liu and Y. Chen, Alternating Nanolayers as Lithiophilic Scaffolds for Li-Metal Anode, *J. Energy Chem.*, 2021, **57**, 131–139, DOI: 10.1016/j.jechem.2020.08.034.

171 R. Javaid, Catalytic Hydrogen Production, Storage and Application, *Catalysts*, 2021, **11**(7), 836.

172 E. B. Agyekum, C. Nutakor, A. M. Agwa and S. Kamel, A Critical Review of Renewable Hydrogen Production Methods: Factors Affecting Their Scale-up and Its Role in Future Energy Generation, *Membranes*, 2022, **12**(2), 173.

173 Y. Yang, J. Liu, M. Gu, B. Cheng, L. Wang and J. Yu, Bifunctional TiO2/COF S-Scheme Photocatalyst with Enhanced H2O2 Production and Furoic Acid Synthesis Mechanism, *Appl. Catal., B*, 2023, **333**, 122780.

174 W. Sun, S. Yang, Y. Liu, C. Shi, W. Shi, X. Lin, F. Guo and Y. Hong, Fabricating Nitrogen-Doped Carbon Dots (NCDs) on Bi3. 64Mo0. 36O6. 55 Nanospheres: A Nanoheterostructure for Enhanced Photocatalytic Performance for Water Purification, *J. Phys. Chem. Solids*, 2021, **159**, 110283.

175 W. Zhao, Z. Chen, X. Yang, X. Qian, C. Liu, D. Zhou, T. Sun, M. Zhang, G. Wei and P. D. Dissanayake, Recent Advances in Photocatalytic Hydrogen Evolution with High-Performance Catalysts without Precious Metals, *Renewable Sustainable Energy Rev.*, 2020, **132**, 110040.

176 J. Liu, P. Wang, J. Fan, H. Yu and J. Yu, In Situ Synthesis of Mo2C Nanoparticles on Graphene Nanosheets for Enhanced Photocatalytic H2-Production Activity of TiO2, *ACS Sustainable Chem. Eng.*, 2021, **9**(10), 3828–3837, DOI: 10.1021/acssuschemeng.0c08903.

177 T. Song, B. Long, S. Yin, A. Ali and G.-J. Deng, Designed Synthesis of a Porous Ultrathin 2D CN@graphene@CN Sandwich Structure for Superior Photocatalytic Hydrogen Evolution under Visible Light, *Chem. Eng. J.*, 2021, **404**, 126455, DOI: 10.1016/j.cej.2020.126455.

178 H. Boumeriame, B. F. Machado, N. M. M. Moura, P. Serp, L. Andrade, T. Lopes, A. Mendes, T. Chafik, E. S. Da Silva and J. L. Faria, Graphitic Carbon Nitride/Few-Layer Graphene Heterostructures for Enhanced Visible-LED Photocatalytic Hydrogen Generation, *Int. J. Hydrogen Energy*, 2022, **47**(61), 25555–25570, DOI: 10.1016/j.ijhydene.2022.05.285.

179 L. K. Putri, B.-J. Ng, W.-J. Ong, H. W. Lee, W. S. Chang, A. R. Mohamed and S.-P. Chai, Energy Level Tuning of CdSe Colloidal Quantum Dots in Ternary 0D-2D-2D CdSe QD/B-rGO/O-gC3N4 as Photocatalysts for Enhanced Hydrogen Generation, *Appl. Catal., B*, 2020, **265**, 118592, DOI: 10.1016/j.apcatb.2020.118592.

180 J.-Q. Yan, W. Peng, S.-S. Zhang, D.-P. Lei and J.-H. Huang, Ternary Ni2P/Reduced Graphene Oxide/g-C3N4 Nanotubes for Visible Light-Driven Photocatalytic H2 Production, *Int. J. Hydrogen Energy*, 2020, **45**(32), 16094–16104, DOI: 10.1016/j.ijhydene.2020.04.001.

181 W. Li, X. Wang, Q. Ma, F. Wang, X. Chu, X. Wang and C. Wang, CdS@h-BN Heterointerface Construction on Reduced Graphene Oxide Nanosheets for Hydrogen Production, *Appl. Catal., B*, 2021, **284**, 119688, DOI: 10.1016/j.apcatb.2020.119688.

182 K. Pramoda, S. Servottam, M. Kaur and C. N. R. Rao, Layered Nanocomposites of Polymer-Functionalized Reduced Graphene Oxide and Borocarbonitride with MoS2 and MoSe2 and Their Hydrogen Evolution Reaction Activity, *ACS Appl. Nano Mater.*, 2020, **3**(2), 1792–1799, DOI: 10.1021/acsanm.9b02482.

183 F. Pan, M. Khan, T. Lei, M. R. Kamli, J. S. M Sabir, I. Khan and M. Z. Ansari, Visible Light Driven Hydrogen Generation and Pollutant Degradation with Au Loaded 2D/2D Heterojunctional Nanocomposite of MoS2 and g-C3N4, *Int. J. Hydrogen Energy*, 2024, **51**, 1141–1153, DOI: 10.1016/j.ijhydene.2023.09.132.

184 K. Namsheer, K. Pramoda, K. S. S. Kumar, S. Radhakrishnan and C. S. Rout, Molybdenum Sulfo-Selenide Nanocomposites with Carbon Nanotubes and Reduced Graphene Oxide for Photocatalytic Hydrogen Evolution Reaction, *Energy Adv.*, 2023, **2**(10), 1724–1734, DOI: 10.1039/D3YA00219E.

185 C. Wang, F. Zheng, L. Zhang, J. Yang and P. Dong, Insight into the Role of Graphene Quantum Dots on the Boosted Photocatalytic H2 Production Performance of a Covalent Organic Framework, *Appl. Surf. Sci.*, 2023, **640**, 158383, DOI: 10.1016/j.apsusc.2023.158383.

186 H. Szalad, A. Uscategui, J. Albero and H. García, 2D/2D Cu-Tetrahydroxyquinone MOF/N-Doped Graphene Heterojunction as Photocatalyst for Overall Water Splitting, *Int. J. Hydrogen Energy*, 2023, **48**(33), 12374–12384, DOI: 10.1016/j.ijhydene.2022.12.168.

187 A. Ejsmont, A. Lewandowska-Andralojc, K. Hauza and J. Goscianska, In Situ Modification of Co-MOF with Graphene Oxide for Enhanced Photocatalytic Hydrogen Production, *Int. J. Hydrogen Energy*, 2023, **48**(24), 8965–8970, DOI: 10.1016/j.ijhydene.2022.12.084.

188 K. Dai, T. Hu, J. Zhang and L. Lu, Carbon Nanotube Exfoliated Porous Reduced Graphene Oxide/CdS-Diethylenetriamine Heterojunction for Efficient Photocatalytic H2 Production, *Appl. Surf. Sci.*, 2020, **512**, 144783, DOI: 10.1016/j.apsusc.2019.144783.

189 H. Shen, M. Wang, X. Zhang, D. Li, G. Liu and W. Shi, 2D/2D/3D Architecture Z-scheme System for Simultaneous H2 Generation and Antibiotic Degradation, *Fuel*, 2020, **280**, 118618, DOI: 10.1016/j.fuel.2020.118618.

190 D. Liu, J. Yao, S. Chen, J. Zhang, R. Li and T. Peng, Construction of rGO-Coupled C3N4/C3N5 2D/2D Z-Scheme Heterojunction to Accelerate Charge Separation for Efficient Visible Light H2 Evolution, *Appl. Catal., B*, 2022, **318**, 121822, DOI: 10.1016/j.apcatb.2022.121822.
191 M. Tahir and N. S. Amin, Advances in Visible Light Responsive Titanium Oxide-Based Photocatalysts for CO2 Conversion to Hydrocarbon Fuels, *Energy Convers. Manage.*, 2013, **76**, 194–214.
192 T. Grewe, M. Meggouh and H. Tueysuez, Nanocatalysts for Solar Water Splitting and a Perspective on Hydrogen Economy, *Chem.–Asian J.*, 2016, **11**(1), 22–42.
193 R. V. Gonçalves, H. Wender, S. Khan and M. A. Melo, Photocatalytic Water Splitting by Suspended Semiconductor Particles, *Nanoenergy: Nanotechnology Applied for Energy Production*, 2018, pp. 107–140.
194 C. Acar, I. Dincer and G. F. Naterer, Review of Photocatalytic Water-splitting Methods for Sustainable Hydrogen Production, *Int. J. Energy Res.*, 2016, **40**(11), 1449–1473.
195 S. Tasleem and M. Tahir, Current Trends in Strategies to Improve Photocatalytic Performance of Perovskites Materials for Solar to Hydrogen Production, *Renewable Sustainable Energy Rev.*, 2020, **132**, 110073.
196 A. Kudo and Y. Miseki, Heterogeneous Photocatalyst Materials for Water Splitting, *Chem. Soc. Rev.*, 2009, **38**(1), 253–278.
197 P. Shandilya, R. Sharma, R. K. Arya, A. Kumar, D.-V. N. Vo and G. Sharma, Recent Progress and Challenges in Photocatalytic Water Splitting Using Layered Double Hydroxides (LDH) Based Nanocomposites, *Int. J. Hydrogen Energy*, 2022, **47**(88), 37438–37475.
198 W. Nabgan, H. Alqaraghuli, A. Owgi, M. Ikram, D.-V. N. Vo, A. A. Jalil, R. Djellabi, A. H. Nordin and F. Medina, A Review on the Design of Nanostructure-Based Materials for Photoelectrochemical Hydrogen Generation from Wastewater: Bibliometric Analysis, Mechanisms, Prospective, and Challenges, *Int. J. Hydrogen Energy*, 2023, **52**, 622–663.
199 X. Li, J. Yu, S. Wageh, A. A. Al-Ghamdi and J. Xie, Graphene in Photocatalysis: A Review, *Small*, 2016, **12**(48), 6640–6696.
200 J. W. Ager, M. R. Shaner, K. A. Walczak, I. D. Sharp and S. Ardo, Experimental Demonstrations of Spontaneous, Solar-Driven Photoelectrochemical Water Splitting, *Energy Environ. Sci.*, 2015, **8**(10), 2811–2824.
201 M. Ahmed and I. Dincer, A Review on Photoelectrochemical Hydrogen Production Systems: Challenges and Future Directions, *Int. J. Hydrogen Energy*, 2019, **44**(5), 2474–2507.
202 S. K. Saraswat, D. D. Rodene and R. B. Gupta, Recent Advancements in Semiconductor Materials for Photoelectrochemical Water Splitting for Hydrogen Production Using Visible Light, *Renewable Sustainable Energy Rev.*, 2018, **89**, 228–248.
203 A. Fujishima and K. Honda, Electrochemical Photolysis of Water at a Semiconductor Electrode, *Nature*, 1972, **238**(5358), 37–38.
204 A. Steinfeld, Solar Hydrogen Production via a Two-Step Water-Splitting Thermochemical Cycle Based on Zn/ZnO Redox Reactions, *Int. J. Hydrogen Energy*, 2002, **27**(6), 611–619.
205 D. Das and T. N. Veziroglu, Advances in Biological Hydrogen Production Processes, *Int. J. Hydrogen Energy*, 2008, **33**(21), 6046–6057.
206 Y. Guan, M. Deng, X. Yu and W. Zhang, Two-Stage Photo-Biological Production of Hydrogen by Marine Green Alga Platymonas Subcordiformis, *Biochem. Eng. J.*, 2004, **19**(1), 69–73.
207 L. Díaz, V. Rodríguez, M. González-Rodríguez, E. Rodríguez-Castellón, M. Algarra, P. Núñez and E. Moretti, M/TiO 2 (M= Fe, Co, Ni, Cu, Zn) Catalysts for Photocatalytic Hydrogen Production under UV and Visible Light Irradiation, *Inorg. Chem. Front.*, 2021, **8**(14), 3491–3500.
208 X. Zhong, Y. Li, H. Wu and R. Xie, Recent Progress in BiVO4-Based Heterojunction Nanomaterials for Photocatalytic Applications, *Mater. Sci. Eng. B*, 2023, **289**, 116278.
209 D. Ma, M. Yin, K. Liang, M. Xue, Y. Fan and Z. Li, Simple Synthesis and Efficient Photocatalytic Hydrogen Production of WO3-WS2 and WO3–WS2–MoS2, *Mater. Sci. Semicond. Process.*, 2023, **167**, 107788.
210 S. Ali and T. Ahmad, Treasure Trove for Efficient Hydrogen Evolution through Water Splitting Using Diverse Perovskite Photocatalysts, *Mater. Today Chem.*, 2023, **29**, 101387.
211 N. S. Reddy, R. Vijitha, B. R. Naidu, K. K. Rao, H. Chang-Sik and K. Venkateswarlu, Benchmarking Recent Advances in Hydrogen Production Using G-C3N4-Based Photocatalysts, *Nano Energy*, 2023, 108402.
212 W. Bai, K. Wu, C. Wu, N. Li, Y. Gao and L. Ge, Interfacial Engineering to Construct 2D-2D NiCo-LDH/g-C3N4 Heterojunctions for Enhanced Photocatalytic Hydrogen Production Performance, *Int. J. Hydrogen Energy*, 2023, **48**(44), 16704–16714.
213 M. Jiang, M. Huang, J. Cong, Y. Yao, W. Sun and B. Wang, Enhanced Visible-Light Photocatalytic Activity of ZrO2/gCN Composite by Introducing Nitrogen Vacancies with H2 Plasma Treatment, *J. Photochem. Photobiol., A*, 2024, **448**, 115324.
214 Z. Qi, J. Chen, Q. Li, N. Wang, S. A. Carabineiro and K. Lv, Increasing the Photocatalytic Hydrogen Generation Activity of CdS Nanorods by Introducing Interfacial and Polarization Electric Fields, *Small*, 2023, **19**(46), 2303318.
215 Q. Mao, J. Chen, H. Chen, Z. Chen, J. Chen and Y. Li, Few-Layered 1T-MoS 2-Modified ZnCoS Solid-Solution Hollow Dodecahedra for Enhanced Photocatalytic Hydrogen Evolution, *J. Mater. Chem. A*, 2019, **7**(14), 8472–8484.
216 L. Wang, J. Zhao, H. Liu and J. Huang, Design, Modification and Application of Semiconductor Photocatalysts, *J. Taiwan Inst. Chem. Eng.*, 2018, **93**, 590–602.
217 S. Chandrappa, D. H. Murthy, N. L. Reddy, S. J. Babu, D. Rangappa, U. Bhargav, V. Preethi, M. M. Kumari and M. V. Shankar, Utilizing 2D Materials to Enhance H2 Generation Efficiency via Photocatalytic Reforming Industrial and Solid Waste, *Environ. Res.*, 2021, **200**, 111239.

218 X. Li, R. Shen, S. Ma, X. Chen and J. Xie, Graphene-Based Heterojunction Photocatalysts, *Appl. Surf. Sci.*, 2018, **430**, 53–107.
219 Q. Xiang, J. Yu and M. Jaroniec, Graphene-Based Semiconductor Photocatalysts, *Chem. Soc. Rev.*, 2012, **41**(2), 782–796.
220 L. Han, P. Wang and S. Dong, Progress in Graphene-Based Photoactive Nanocomposites as a Promising Class of Photocatalyst, *Nanoscale*, 2012, **4**(19), 5814–5825.
221 A. Mondal, A. Prabhakaran, S. Gupta and V. R. Subramanian, Boosting Photocatalytic Activity Using Reduced Graphene Oxide (RGO)/Semiconductor Nanocomposites: Issues and Future Scope, *ACS Omega*, 2021, **6**(13), 8734–8743, DOI: **10.1021/acsomega.0c06045**.
222 J. Corredor, M. J. Rivero and I. Ortiz, New Insights in the Performance and Reuse of rGO/TiO2 Composites for the Photocatalytic Hydrogen Production, *Int. J. Hydrogen Energy*, 2021, **46**(33), 17500–17506, DOI: **10.1016/j.ijhydene.2020.01.181**.
223 F. Khan, M. S. Khan, S. Kamal, M. Arshad, S. I. Ahmad and S. A. Nami, Recent Advances in Graphene Oxide and Reduced Graphene Oxide Based Nanocomposites for the Photodegradation of Dyes, *J. Mater. Chem. C*, 2020, **8**(45), 15940–15955.
224 J. Yu, L. Zhang and P. Kuang, *Graphene Oxide–Metal Oxide and Other Graphene Oxide-Based Composites in Photocatalysis and Electrocatalysis*, Elsevier, 2022.
225 A. N. Ghoti, A. B. Patil and S. K. Pardeshi, Li Sensitized CdS/TiO2 Nanocomposite Photoanode for Solar Water Splitting, Hydrogen Generation and Photoelectrochemical (PEC) Performance, *Int. J. Hydrogen Energy*, 2024, **51**, 1586–1597.
226 L. Huang, L. He, J. Ni, H. Liu, Z. Xu, C. Gong, Q. Zhang and B. Zhang, WO3/Mo: BiVO4 Heterojunction Structured Photoelectrochemical Sensor for Enhancing Hydrogen Peroxide Monitoring and Mechanism Investigation, *Electrochim. Acta*, 2023, **439**, 141641.
227 Z. Masoumi, M. Tayebi, M. Kolaei and B.-K. Lee, Improvement of Surface Light Absorption of ZnO Photoanode Using a Double Heterojunction with α–Fe2O3/g–C3N4 Composite to Enhance Photoelectrochemical Water Splitting, *Appl. Surf. Sci.*, 2023, **608**, 154915, DOI: **10.1016/j.apsusc.2022.154915**.
228 A. Z. Khan, T. A. Kandiel, S. Abdel-Azeim, T. N. Jahangir and K. Alhooshani, Phosphate Ions Interfacial Drift Layer to Improve the Performance of CoFe−Prussian Blue Hematite Photoanode toward Water Splitting, *Appl. Catal., B*, 2022, **304**, 121014, DOI: **10.1016/j.apcatb.2021.121014**.
229 L. Fu, Z. Li and X. Shang, Recent Surficial Modification Strategies on BiVO4 Based Photoanodes for Photoelectrochemical Water Splitting Enhancement, *Int. J. Hydrogen Energy*, 2024, **55**, 611–624, DOI: **10.1016/j.ijhydene.2023.11.253**.
230 Q. Wang, Y. Zhang, Y. Liu, K. Wang, W. Qiu, L. Chen, W. Li and J. Li, Photocorrosion Behavior of Cu2O Nanowires during Photoelectrochemical CO2 Reduction, *J. Electroanal. Chem.*, 2022, **912**, 116252, DOI: **10.1016/j.jelechem.2022.116252**.
231 R. Chong, Z. Wang, J. Lv, J. Rong, L. Zhang, Y. Jia, L. Wang, Z. Chang and X. Wang, A Hybrid CoOOH-rGO/Fe2O3 Photoanode with Spatial Charge Separation and Charge Transfer for Efficient Photoelectrochemical Water Oxidation, *J. Catal.*, 2021, **399**, 170–181, DOI: **10.1016/j.jcat.2021.05.006**.
232 L. Li, B. Li, H. Liu, M. Li and B. Wang, Photoelectrochemical Sensing of Hydrogen Peroxide Using TiO2 Nanotube Arrays Decorated with RGO/CdS, *J. Alloys Compd.*, 2020, **815**, 152241, DOI: **10.1016/j.jallcom.2019.152241**.
233 S. Vigneshwaran, P. Karthikeyan, C. M. Park and S. Meenakshi, Boosted Insights of Novel Accordion-like (2D/2D) Hybrid Photocatalyst for the Removal of Cationic Dyes: Mechanistic and Degradation Pathways, *J. Environ. Manage.*, 2020, **273**, 111125, DOI: **10.1016/j.jenvman.2020.111125**.
234 D. Vidyasagar, A. Gupta, A. Balapure, S. G. Ghugal, A. G. Shende and S. S. Umare, 2D/2D Wg-C3N4/g-C3N4 Composite as "Adsorb and Shuttle" Model Photocatalyst for Pollution Mitigation, *J. Photochem. Photobiol., A*, 2019, **370**, 117–126, DOI: **10.1016/j.jphotochem.2018.10.038**.
235 H. Che, G. Che, H. Dong, W. Hu, H. Hu, C. Liu and C. Li, Fabrication of Z-Scheme Bi3O4Cl/g-C3N4 2D/2D Heterojunctions with Enhanced Interfacial Charge Separation and Photocatalytic Degradation Various Organic Pollutants Activity, *Appl. Surf. Sci.*, 2018, **455**, 705–716, DOI: **10.1016/j.apsusc.2018.06.038**.
236 B. Miao, Y. Zhang, Q. Chen, Y. Zhang, Y. Cao, Z. Bai and L. Chen, Highly Enhanced Photocatalytic Hydrogen Production Performance of Heterostructured Ti3C2/TiO2/rGO Composites, *Langmuir*, 2022, **38**(50), 15579–15591, DOI: **10.1021/acs.langmuir.2c02227**.
237 S. Nayak and K. Parida, Recent Progress in LDH@Graphene and Analogous Heterostructures for Highly Active and Stable Photocatalytic and Photoelectrochemical Water Splitting, *Chem.–Asian J.*, 2021, **16**(16), 2211–2248.
238 D.-B. Seo, T. N. Trung, D.-O. Kim, D. V. Duc, S. Hong, Y. Sohn, J.-R. Jeong and E.-T. Kim, Plasmonic Ag-Decorated Few-Layer MoS 2 Nanosheets Vertically Grown on Graphene for Efficient Photoelectrochemical Water Splitting, *Nano-Micro Lett.*, 2020, **12**, 1–14.
239 F. Carraro, L. Calvillo, M. Cattelan, M. Favaro, M. Righetto, S. Nappini, I. Píš, V. Celorrio, D. J. Fermín, A. Martucci, S. Agnoli and G. Granozzi, Fast One-Pot Synthesis of MoS2/Crumpled Graphene p–n Nanonjunctions for Enhanced Photoelectrochemical Hydrogen Production, *ACS Appl. Mater. Interfaces*, 2015, **7**(46), 25685–25692, DOI: **10.1021/acsami.5b06668**.
240 Q. Quan, S. Xie, B. Weng, Y. Wang and Y. Xu, Revealing the Double-Edged Sword Role of Graphene on Boosted Charge Transfer versus Active Site Control in TiO2 Nanotube Arrays@ RGO/MoS2 Heterostructure, *Small*, 2018, **14**(21), 1704531.

241 S. R. Gujjula, U. Pal, N. Chanda, S. Karingula, S. Chirra, S. Siliveri, S. Goskula and V. Narayanan, Versatile Bifunctional Ag@g-C3N4/r-GO Catalyst for Efficient Photo- and Electrocatalytic H2 Production, *Energy Fuels*, 2023, **37**(13), 9722–9735, DOI: **10.1021/acs.energyfuels.3c00518**.

242 M. Nasr, L. Benhamou, A. Kotbi, N. S. Rajput, A. Campos, A.-I. Lahmar, K. Hoummada, K. Kaja, M. El Marssi and M. Jouiad, Photoelectrochemical Enhancement of Graphene@ WS2 Nanosheets for Water Splitting Reaction, *Nanomaterials*, 2022, **12**(11), 1914.

243 A. K. Geim and K. S. Novoselov, The Rise of Graphene, *Nat. Mater.*, 2007, **6**(3), 183–191.

244 K. Jastrzębski and P. Kula, Emerging Technology for a Green, Sustainable Energy-Promising Materials for Hydrogen Storage, from Nanotubes to Graphene—a Review, *Materials*, 2021, **14**(10), 2499.

245 G. Srinivas, Y. Zhu, R. Piner, N. Skipper, M. Ellerby and R. Ruoff, Synthesis of Graphene-like Nanosheets and Their Hydrogen Adsorption Capacity, *Carbon*, 2010, **48**(3), 630–635, DOI: **10.1016/j.carbon.2009.10.003**.

246 C. X. Guo, Y. Wang and C. M. Li, Hierarchical Graphene-Based Material for over 4.0 Wt% Physisorption Hydrogen Storage Capacity, *ACS Sustain. Chem. Eng.*, 2013, **1**(1), 14–18.

247 S. H. Aboutalebi, S. Aminorroaya-Yamini, I. Nevirkovets, K. Konstantinov and H. K. Liu, Enhanced Hydrogen Storage in Graphene oxide-MWCNTs Composite at Room Temperature, *Adv. Energy Mater.*, 2012, **2**(12), 1439–1446.

248 V. Jain and B. Kandasubramanian, Functionalized Graphene Materials for Hydrogen Storage, *J. Mater. Sci.*, 2020, **55**(5), 1865–1903.

249 C.-C. Huang, N.-W. Pu, C.-A. Wang, J.-C. Huang, Y. Sung and M.-D. Ger, Hydrogen Storage in Graphene Decorated with Pd and Pt Nano-Particles Using an Electroless Deposition Technique, *Sep. Purif. Technol.*, 2011, **82**, 210–215.

250 V. B. Parambhath, R. Nagar and S. Ramaprabhu, Effect of Nitrogen Doping on Hydrogen Storage Capacity of Palladium Decorated Graphene, *Langmuir*, 2012, **28**(20), 7826–7833.

251 A. Ariharan, B. Viswanathan and V. Nandhakumar, Nitrogen Doped Graphene as Potential Material for Hydrogen Storage, *Graphene*, 2017, **6**(2), 41–60.

252 J. Hao, F. Wei, X. Zhang, L. Li, C. Chen, G. Wu, L. Wu, D. Liang, X. Ma, P. Lu and H. Song, An Investigation of Li-Decorated N-Doped Penta-Graphene for Hydrogen Storage, *Int. J. Hydrogen Energy*, 2021, **46**(50), 25533–25542, DOI: **10.1016/j.ijhydene.2021.05.089**.

253 S. S. Samantaray, V. Sangeetha, S. Abinaya and S. Ramaprabhu, Enhanced Hydrogen Storage Performance in Pd3Co Decorated Nitrogen/Boron Doped Graphene Composites, *Int. J. Hydrogen Energy*, 2018, **43**(16), 8018–8025, DOI: **10.1016/j.ijhydene.2018.03.078**.

254 Y. Gao, H. Zhang, H. Pan, Q. Li and J. Zhao, Ultrahigh Hydrogen Storage Capacity of Holey Graphyne, *Nanotechnology*, 2021, **32**(21), 215402, DOI: **10.1088/1361-6528/abe48d**.

255 J. Dewangan, V. Mahamiya, A. Shukla and B. Chakraborty, Lithium Decorated ψ-Graphene as a Potential Hydrogen Storage Material: Density Functional Theory Investigations, *Int. J. Hydrogen Energy*, 2023, **48**(96), 37908–37920, DOI: **10.1016/j.ijhydene.2022.10.142**.

256 B. Chakraborty, P. Ray, N. Garg and S. Banerjee, High Capacity Reversible Hydrogen Storage in Titanium Doped 2D Carbon Allotrope ψ-Graphene: Density Functional Theory Investigations, *Int. J. Hydrogen Energy*, 2021, **46**(5), 4154–4167, DOI: **10.1016/j.ijhydene.2020.10.161**.

257 H. T. Nair, P. K. Jha and B. Chakraborty, High-Capacity Hydrogen Storage in Zirconium Decorated Psi-Graphene: Acumen from Density Functional Theory and Molecular Dynamics Simulations, *Int. J. Hydrogen Energy*, 2023, **48**(96), 37860–37871, DOI: **10.1016/j.ijhydene.2022.08.084**.

258 M. Singh, A. Shukla and B. Chakraborty, High Capacity Hydrogen Storage on Zirconium Decorated γ-Graphyne: A Systematic First-Principles Study, *Int. J. Hydrogen Energy*, 2023, **48**(96), 37834–37846, DOI: **10.1016/j.ijhydene.2022.07.062**.

259 P. Panigrahi, M. Desai, M. K. Talari, H. Bae, H. Lee, R. Ahuja and T. Hussain, Selective Decoration of Nitrogenated Holey Graphene (C2N) with Titanium Clusters for Enhanced Hydrogen Storage Application, *Int. J. Hydrogen Energy*, 2021, **46**(10), 7371–7380, DOI: **10.1016/j.ijhydene.2020.11.222**.

260 Y. Chen, H. Habibullah, G. Xia, C. Jin, Y. Wang, Y. Yan, Y. Chen, X. Gong, Y. Lai and C. Wu, Palladium-Phosphide-Modified Three-Dimensional Phospho-Doped Graphene Materials for Hydrogen Storage, *Materials*, 2023, **16**(12), 4219.

261 S. Dong, E. Lv, J. Wang, C. Li, K. Ma, Z. Gao, W. Yang, Z. Ding, C. Wu and I. D. Gates, Construction of Transition Metal-Decorated Boron Doped Twin-Graphene for Hydrogen Storage: A Theoretical Prediction, *Fuel*, 2021, **304**, 121351, DOI: **10.1016/j.fuel.2021.121351**.

262 C. U. Deniz, H. Mert and C. Baykasoglu, Li-Doped Fullerene Pillared Graphene Nanocomposites for Enhancing Hydrogen Storage: A Computational Study, *Comput. Mater. Sci.*, 2021, **186**, 110023, DOI: **10.1016/j.commatsci.2020.110023**.

263 Y. Chen, H. Habibullah, G. Xia, C. Jin, Y. Wang, Y. Yan, Y. Chen, X. Gong, Y. Lai and C. Wu, Hydrogen Storage Properties of Economical Graphene Materials Modified by Non-Precious Metal Nickel and Low-Content Palladium, *Inorganics*, 2023, **11**(6), 251.

264 A. L. Triguero and S. Rezaie, *Hydrogen Storage Performance of an Au-Decorated Graphene Nanosheet*, 2022.

265 S. S. Samantaray, V. Sangeetha, S. Abinaya and S. Ramaprabhu, Diatom Frustule-Graphene Based Nanomaterial for Room Temperature Hydrogen Storage, *Int. J. Hydrogen Energy*, 2020, **45**(1), 764–773, DOI: **10.1016/j.ijhydene.2019.10.155**.

266 R. Nagar, B. P. Vinayan, S. S. Samantaray and S. Ramaprabhu, Recent Advances in Hydrogen Storage

Using Catalytically and Chemically Modified Graphene Nanocomposites, *J. Mater. Chem. A*, 2017, **5**(44), 22897–22912, DOI: **10.1039/C7TA05068B**.

267 D. Zhou, C. Zheng, Y. Niu, D. Feng, H. Ren, Y. Zhang and H. Yu, Hydrogen Storage Property Improvement of Ball-Milled Mg2.3Y0.1Ni Alloy with Graphene, *Int. J. Hydrogen Energy*, 2024, **50**, 123–135, DOI: **10.1016/j.ijhydene.2023.06.255**.

268 S. Gulati, Mansi, S. Vijayan, S. Kumar, V. Agarwal, B. Harikumar and R. S. Varma, Magnetic Nanocarriers Adorned on Graphene: Promising Contrast-Enhancing Agents with State-of-the-Art Performance in Magnetic Resonance Imaging (MRI) and Theranostics, *Mater. Adv.*, 2022, **3**(7), 2971–2989, DOI: **10.1039/D1MA01071A**.